Article

Global prevalence of non-perennial rivers and streams

https://doi.org/10.1038/s41586-021-03565-5

Received: 12 November 2020

Accepted: 19 April 2021

Published online: 16 June 2021

Check for updates

Mathis Loïc Messager[1,2]✉, Bernhard Lehner[1]✉, Charlotte Cockburn[1,7], Nicolas Lamouroux[2], Hervé Pella[2], Ton Snelder[3], Klement Tockner[4,5], Tim Trautmann[6], Caitlin Watt[1,8] & Thibault Datry[2]✉

Flowing waters have a unique role in supporting global biodiversity, biogeochemical cycles and human societies[1–5]. Although the importance of permanent watercourses is well recognized, the prevalence, value and fate of non-perennial rivers and streams that periodically cease to flow tend to be overlooked, if not ignored[6–8]. This oversight contributes to the degradation of the main source of water and livelihood for millions of people[5]. Here we predict that water ceases to flow for at least one day per year along 51–60 per cent of the world's rivers by length, demonstrating that non-perennial rivers and streams are the rule rather than the exception on Earth. Leveraging global information on the hydrology, climate, geology and surrounding land cover of the Earth's river network, we show that non-perennial rivers occur within all climates and biomes, and on every continent. Our findings challenge the assumptions underpinning foundational river concepts across scientific disciplines[9]. To understand and adequately manage the world's flowing waters, their biodiversity and functional integrity, a paradigm shift is needed towards a new conceptual model of rivers that includes flow intermittence. By mapping the distribution of non-perennial rivers and streams, we provide a stepping-stone towards addressing this grand challenge in freshwater science.

Almost every river network on Earth includes channels that periodically cease to flow. From Himalayan snow-fed creeks to occasionally water-filled Saharan wadis, river flow cessation is naturally prevalent worldwide. Yet the global extent of intermittent rivers and ephemeral streams (IRES) is largely unknown. IRES vary widely in size and flow duration, encompassing all non-perennial watercourses—from large, rarely intermittent rivers with nearly continuous channel flow to mostly dry streams that only flow after intense rainfall (see Extended Data Table 1 for additional definitions and IRES terminology). IRES are pivotal components of the landscape, critically contributing to the biodiversity[1,2], biogeochemical processes and functional integrity of fluvial systems[3,4]. Many formerly perennial rivers and streams have become intermittent in the past 50 years owing to water abstractions, climate change and land use transitions, including sections of iconic rivers such as the Nile, Indus, Yellow and Colorado[10,11]. Given continued global change, an increasingly large proportion of the global river network is expected to seasonally cease to flow over the coming decades[12,13].

Despite their prevalence, IRES are frequently mismanaged owing to a lack of recognition[6], or altogether excluded from management actions and conservation laws[7]. As a result, non-perennial rivers and streams are being degraded at an alarming rate[6]. Recent attempts to further remove IRES from environmental legislation and national water governance systems (for example, in the USA[8]), if implemented, would worsen their already inadequate protection. The long-standing neglect of IRES is partly the result of their continued omission from scientific research. Most freshwater science has focused on the functioning and conservation of perennial water bodies, and only recently has riverine flow cessation become its own subject of study[1,9,10]. Consequently, science-based methods for managing these unique ecosystems, such as biomonitoring tools and protocols, are still limited or absent[5,14]. Management frameworks also need to be adapted to conserve environmental flows in IRES[15]—that is, the quantity, timing, and quality of freshwater flows necessary to sustain aquatic ecosystems and their associated benefits[16]. But perhaps the most important gap until now has been our inability to quantify and map IRES worldwide. Accurate mapping of non-perennial rivers and streams would provide crucial baseline information to determine and monitor their role in biogeochemical and water cycles and in supporting global biological diversity[3].

Streamflow monitoring data for IRES are scant, spatially biased, and of uneven quality[17]. Indeed, most streamflow gauging stations are installed on large, perennial rivers worldwide[17]. The dearth of primary data has triggered the development of alternative methods to map IRES, including citizen science or expert field observations of streamflow state, in situ sensor networks and remote sensing[18–20]. However, these efforts only provide information at local scales and suffer from several limitations (for example, remote sensing of smaller rivers can

[1]Department of Geography, McGill University, Montreal, Quebec, Canada. [2]RiverLY Research Unit, National Research Institute for Agriculture, Food and Environment (INRAE), Villeurbanne, France. [3]LWP Ltd, Christchurch, New Zealand. [4]Senckenberg Society for Nature Research, Frankfurt am Main, Germany. [5]Faculty of Biological Sciences, Goethe University Frankfurt, Frankfurt am Main, Germany. [6]Institute of Physical Geography, Goethe University Frankfurt, Frankfurt am Main, Germany. [7]Present address: Department of Earth Science, Dartmouth College, Hanover, NH, USA. [8]Present address: Lethbridge Research and Development Centre, Agriculture and Agri-Food Canada, Lethbridge, Alberta, Canada. ✉e-mail: mathis.messager@mail.mcgill.ca; bernhard.lehner@mcgill.ca; thibault.datry@inrae.fr

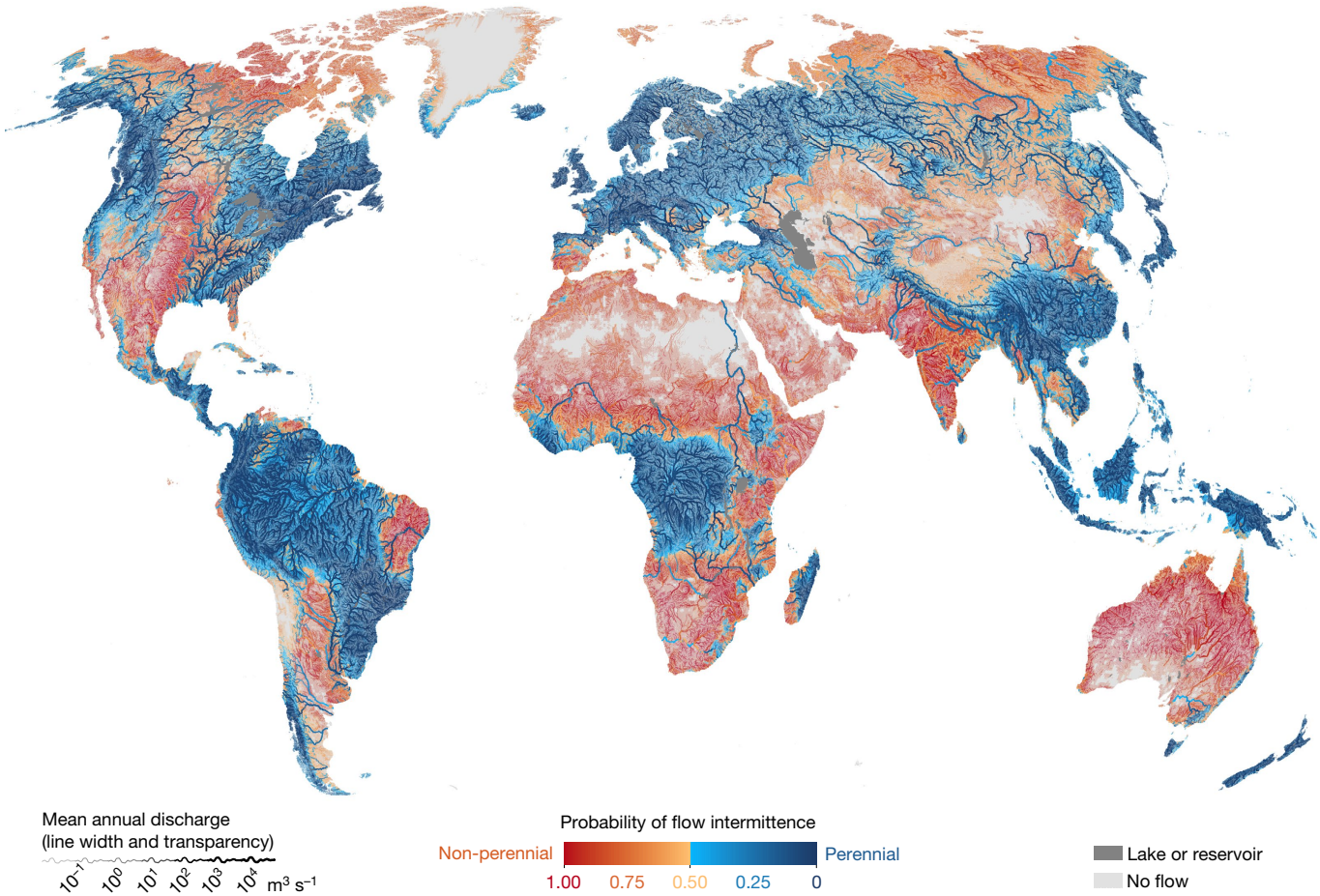

Fig. 1 | Global distribution of non-perennial rivers and streams. Intermittence is defined as flow cessation for at least one day per year on average. The median probability threshold of 0.5 was used to determine the binary flow intermittence class for each reach in RiverATLAS[27]. Mapping software: ArcMap (ESRI).

be obstructed by overhanging riparian vegetation and cloud cover[20]). Model-based classifications of river types, either IRES-focused (for example, in mainland France[21], the north-western USA[22], eastern Australia[23]) or general (for example, Australia[24], California[25]), have also provided important baseline estimates of the spatial distribution of IRES from the catchment to the national scale. However, a rigorous estimation of the global prevalence and distribution of IRES is still lacking.

In this study, we developed a statistical random forest (RF) model (see Methods for details) to produce the first reach-scale estimate of the distribution of IRES for the 23.3 million kilometres of mapped rivers and streams across the globe (except Antarctica) whose long-term average naturalized discharge exceeds 0.1 $m^3 s^{-1}$, and then extrapolated our IRES estimates to the nearly 64 million kilometres of rivers and streams with an average discharge higher than 0.01 $m^3 s^{-1}$. For this purpose, we linked quality-checked observed streamflow data from 5,615 gauging stations (on 4,428 perennial and 1,187 non-perennial reaches) with 113 candidate environmental predictors available globally (Extended Data Table 2). Predictors included variables describing climate, physiography, land cover, soil, geology and groundwater, as well as estimates of long-term naturalized (that is, without anthropogenic water use in the form of abstractions or impoundments) mean monthly and mean annual flow (MAF), derived from a global hydrological model (WaterGAP 2.2)[26]. Following model training and validation, we predicted the probability of flow intermittence for all river reaches in the RiverATLAS database[27], a digital representation of the global river network at high spatial resolution.

Prevalence and distribution of IRES

We predict that water ceases to flow for at least one day per year, on interannual average, along 41% of the mapped global river network length, that is, all rivers and streams with MAF ≥ 0.1 $m^3 s^{-1}$ (Fig. 1, Table 1). However, any estimate of the percentage of IRES reaches in a river system, whether for a small catchment or for the globe, is inherently dependent on cartographic scale. Although many dryland rivers exhibit downstream decreases in discharge owing to channel evaporation and transmission losses[28], river flow tends to become more permanent with increasing drainage area and distance from the headwaters in a basin[29], which is well reflected in the predictions of our model. Because of the dendritic nature of river networks, small headwater streams, which are more prone to intermittence, make up a greater proportion of the total stream length than larger downstream rivers[30]. Consequently, the percentage of the river network length that is non-perennial increases with decreasing size of the smallest mapped stream. To account for this distribution, we made a first-order approximation of the prevalence of intermittence in small streams by extrapolating our estimate to streams with 0.01 $m^3 s^{-1}$ ≤ MAF < 0.1 $m^3 s^{-1}$ (see Methods for details). Including this size class, we estimate that 60% of all rivers and streams globally are IRES; and we found a lower bound of this estimate at 51% after applying an alternative, more conservative extrapolation approach. This demonstrates that IRES represent the world's most widespread type of rivers.

For river flow to occur, water from rainfall, snowmelt, or releases from existing storage (for example, lakes, reservoirs, groundwater) must exceed losses from infiltration and evapotranspiration[31]. Climatic

Table 1 | Global prevalence of IRES across climate zones and streamflow size classes

Climate zone[a]	Prevalence of intermittence (% of network length) by streamflow size class ($m^3 s^{-1}$)							Total intermittence (% length)	Total stream length[b] ($\times 10^3$ km)
	Extrapolated[c]	Mapped						Including | (excluding) extrapolated stream class[c]	
	[10^{-2}, 10^{-1})	[10^{-1}, 1)	[1, 10)	[10, 10^2)	[10^2, 10^3)	[10^3, 10^4)	≥10^4		
Extremely hot and arid	*100*	100	100	98	49	0	–	99 | (98)	1,032 | (249)
Hot and arid	*100*	100	100	97	46	0	–	99 | (98)	990 | (238)
Arctic 1	*100*	92	71	100	–	–	–	96 | (92)	11 | (6)
Warm temperate and xeric	*99*	96	89	59	11	0	0	96 | (89)	1,351 | (444)
Extremely cold and wet 2	*100*	93	69	34	0	–	–	96 | (87)	766 | (243)
Extremely hot and xeric	*99*	90	95	90	45	0	0	95 | (89)	4,551 | (1,605)
Arctic 2	*100*	89	18	8	–	–	–	92 | (82)	98 | (41)
Cool temperate and xeric	*94*	81	70	37	2	0	–	87 | (72)	1,709 | (552)
Extremely cold and mesic	*96*	70	45	34	26	22	0	83 | (61)	8,083 | (3,051)
Extremely cold and wet 1	*92*	59	10	1	0	–	–	72 | (50)	227 | (109)
Cold and mesic	*90*	47	26	6	3	0	0	70 | (37)	8,189 | (3,084)
Warm temperate and mesic	*84*	45	35	16	1	0	0	63 | (39)	3,582 | (1,646)
Hot and dry	*77*	47	36	23	7	0	0	62 | (41)	4,054 | (1,683)
Cool temperate and dry	*65*	46	34	11	0	0	0	57 | (39)	4,087 | (1,325)
Hot and mesic	*77*	30	24	23	5	0	0	54 | (27)	4,452 | (2,023)
Extremely hot and moist	*35*	18	20	21	4	0	0	30 | (18)	19,117 | (6,002)
Cool temperate and moist	*52*	18	10	0	0	0	–	29 | (13)	1,164 | (691)
Cold and wet	*34*	1	0	0	0	0	–	14 | (1)	493 | (299)
World	***70***	**47**	**35**	**26**	**9**	**1**	**0**	**60 | (41)**	**63,956 | (23,291)**

[a]Global Environmental Stratification (GEnS)[32], see Extended Data Fig. 1a.

[b]Excluding sections of river reaches contained within a lake.

[c]Extrapolated statistics based on the main estimate (as opposed to the lower-bound estimate, see Methods for details).

variables, in particular climate-induced aridity, were therefore the leading predictors of river flow cessation and the occurrence of IRES (Fig. 2). Our model indicates that where evaporation rates considerably exceed precipitation for at least part of the year, as expressed by a low aridity index (that is, the ratio of mean annual precipitation to mean annual potential evapotranspiration), river networks comprise large proportions of IRES. In extremely hot and xeric environments, which cover nearly one-tenth of the global landmass and encompass most of India, northern Australia and the Sahel region of Africa (see Extended Data Fig. 1a for the global typology of bioclimates[32]), 95% of the river and stream network length is prone to flow cessation (MAF ≥ 0.01 $m^3 s^{-1}$; Table 1). In these environments, we find that even the main stem of major rivers, such as the Niger or Godavari, can dry out.

Outside of arid regions, flow in river networks is primarily controlled by catchment processes influenced by interacting climate and basin conditions[1,29]. In cold climates, for instance, a combination of scarce precipitation, its storage as snow during winter months, and completely freezing streams[33] can lead to high prevalence of flow intermittence. Although not mapped in our study, even streams in Antarctica are known to flow intermittently owing to seasonal patterns of freezing, thawing and/or drying[1]. In humid and temperate regions, IRES are concentrated in the upper end of channel networks where small drainage areas and steep slopes lead to rapid delivery of water to and through the river channel, causing a lack of buffering from variations in precipitation[34]. Therefore, even in the wettest climates (for example, extremely hot and moist; Extended Data Fig. 1a), up to 35% of headwater streams are non-perennial (Table 1). In lowland and large basins, temporary storage and subsequent attenuated release from groundwater, lakes and wetlands, as well as the averaging of local hydrologic variability across a larger drainage area lead to more balanced, steady and thus perennial flow[29].

Our study presents a novel, empirically grounded effort to specifically quantify the prevalence of flow intermittence of rivers and streams globally, and to show that IRES occur across all climates and biomes, and on every continent (Fig. 1, Table 1). Previous assessments reported from 29% to 36% of the global length of rivers to be non-perennial[28,35,36], with inferred and extrapolated estimates exceeding 50%[10,37]. However, these estimates were either generalized hypotheses (for example, based on the global distribution of drylands[28]), geographically constrained (that is, south of 60° N[35–37]), or research by-products within larger projects (for example, using a regional extrapolation to remove IRES from estimates of the global CO_2 emissions of inland waters[37]), rather than dedicated global IRES quantification efforts, and are therefore not directly comparable to our predictions. The FAO AQUAMAPS[35] and GRIN[36] global river networks, for instance, assume that streamflow cessation only occurs in arid and semi-arid areas. See Supplementary Information section I for a review of how previous estimates relate to our predictions, including maps of AQUAMAPS and GRIN estimates.

Our study improves on these previous estimates because it represents diverse hydrometeorological processes beyond aridity at the river reach scale (rather than at the basin scale[37]) by leveraging extensive, high-resolution global data on the hydrology, climate, physiography, geology and surrounding land cover of the world's river network. Furthermore, our study uses global empirical streamflow data for training and validation, which enabled our model to make fine-grained predictions of the intermittence class of rivers across all climates.

Model performance and uncertainties

Performance analysis showed that our RF model could predict the binary flow intermittence class of streamflow gauging stations with high confidence. Cross-validation yielded an overall classification accuracy (the percentage of correctly classified gauges), ranging from 90% to 92% (depending on cross-validation method), and indicated that model predictions were unbiased globally—that is, adequately reflecting the

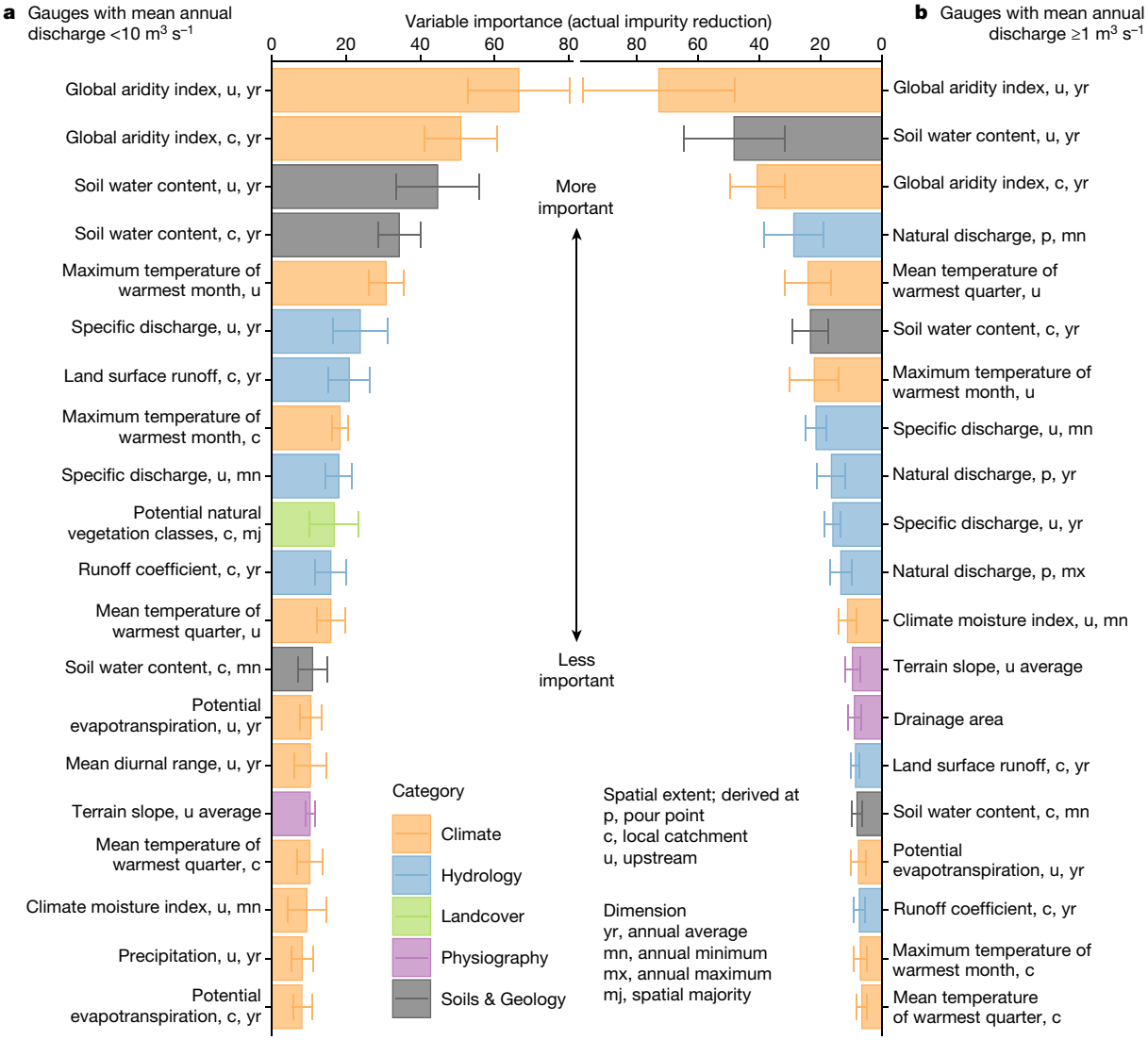

Fig. 2 | Climate-induced aridity and hydrologic variables are the main predictors of global flow intermittence. a, **b**, The two sets of ranked predictor variables represent results from a split random forest model trained on gauges with a mean annual naturalized flow <10 $m^3 s^{-1}$ (**a**) and gauges with a mean annual naturalized flow ≥1 $m^3 s^{-1}$ (**b**). See Methods section 'Machine learning models' for details on model structure and implementation. Rectangular bars show the balanced accuracy-weighted average of actual impurity reduction[49] (AIR) across non-spatial cross-validation folds and repetitions. The longer the bar (that is, the higher the AIR), the more important the variable in predicting flow intermittence. Error brackets show ± one weighted standard deviation of AIR. After the variables' names, the first abbreviation denotes each variable's spatial extent: p (derived at the pour point of the river reach), c (derived within the local catchment that drains directly into the reach), or u (derived within the total drainage area upstream of the reach pour point). The second abbreviation denotes each variable's dimension: yr (annual average), mn (annual minimum), mx (annual maximum), or mj (spatial majority). See Methods and Extended Data Table 2 for data sources of variables.

proportion of IRES gauges in the training dataset. In general, sparsely gauged basins exhibit lower accuracy and higher bias (Fig. 3; for example, in Africa and the Arctic). Boundary areas between climate zones, from mainly non-perennial regions to mainly perennial regions, are also characterized by higher misclassification rates (Extended Data Fig. 2). See Fig. 3 as well as Extended Data Table 3 for cross-validation results.

Our model is based on an inclusive definition of IRES as those rivers and streams that cease to flow at least one day per year on average. To test the sensitivity of our results to the specific threshold of cessation length, we adapted our model and found that 44–53% of the global river network ceases to flow at least one month per year (lower-bound and main estimate, respectively, with MAF ≥ 0.01 $m^3 s^{-1}$; see Methods; Extended Data Fig. 1b, c).

Comparisons with national hydrographic datasets that include information on flow intermittence show that our model predicts a substantially higher prevalence of IRES in the contiguous USA than mapped in the country's atlas (by 31 percentage points), but coincides well with the patterns and extents depicted in the Australian, Argentinian and Brazilian atlases, and with model-generated maps[21] in mainland France (Extended Data Figs. 3–5). The divergence observed in the USA (and to a limited extent in Australia) largely stems from the thresholds used to define IRES—when applying a minimum of one zero-flow month per year, our predictions more closely concur with the comparison dataset (Extended Data Figs. 3, 5).

At an even more local scale, comparing our model predictions against datasets of ground observation points of flow cessation for the US Pacific Northwest and mainland France reveals particular challenges in predicting flow intermittence for small rivers and streams (median MAF ≈ 0.5 $m^3 s^{-1}$, Extended Data Fig. 6). Our model only achieved a balanced accuracy of 0.59 for mainland France (n = 2,297) and of 0.47 for the US Pacific Northwest (n = 3,725), both under- and overestimating

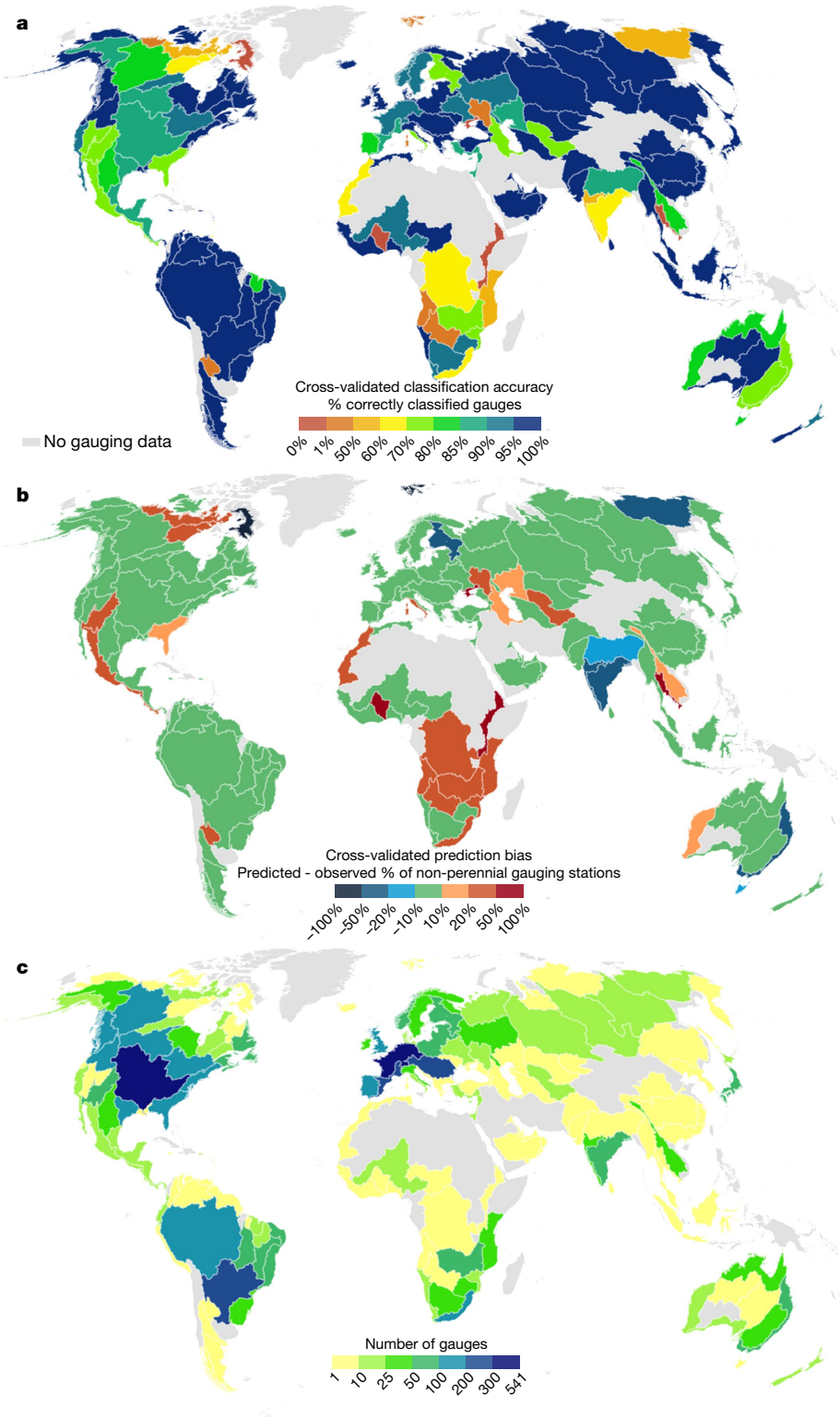

Fig. 3 | Flow intermittence classification accuracy decreases and prediction bias increases in river basins with fewer streamflow gauging stations. a–**c**, Maps of classification accuracy (**a**) and prediction bias (**b**) based on 40-fold spatial cross-validation, and number of streamflow gauging stations per river basin (**c**). See Supplementary Fig. 3 for the distribution of cross-validation folds. River basins correspond to BasinATLAS[27] level 3 subdivisions with an average surface area of 4.6×10^5 km^2. Mapping software: ArcMap (ESRI).

reported IRES, respectively. We hypothesize that heavy water abstractions for domestic and agricultural use are the main reason for the greater contemporary prevalence of intermittence observed in France[38] (from 2012 to 2019) than predicted by our model, which aims to depict the natural distribution of IRES. In the US Pacific Northwest, a lower frequency of observations per site may have led to an underestimation of the prevalence of IRES in the comparison dataset, since the probability of observing a no-flow event increases with the number

of observations. In addition, the mountainous landscape of the region is characterized by complex, local hydrological processes associated with snow and groundwater dynamics that our model can only superficially represent[22].

Despite the increasing uncertainties at national and local scales, the global validation findings demonstrate that our overall statistics and large-scale representation of the spatial distribution of IRES are robust. However, we advise caution in using our model outputs to interpret fine-scale variations in intermittence for small spatial units or for small rivers and streams. The quality of our model results is constrained by the resolution of the river network and associated hydro-environmental predictor variables (250–1,000 m grid cells for most predictors)[27]. Accurate, fine-scale data on catchment soil types and lithology (for example, karst areas), riverbed sediments and groundwater dynamics would be needed to capture variation in the processes influencing flow intermittence at the sub-catchment and reach scales[29]. Groundwater–surface water interaction in particular is an enduring challenge in global hydrological modelling[39] and represents a key process that is only partly represented in our analysis. Also, potential local biases in training data (such as IRES being inconsistently represented in streamflow gauging networks) introduce uncertainties. For instance, model predictions in the south-eastern USA may overestimate the prevalence of IRES, owing to the relative scarcity of gauging stations for model training on small, perennial watercourses in that region. Similarly, the general under- and misrepresentation of small watercourses and arid regions in the global hydrometric network[17] causes substantial difficulty in consistently predicting the prevalence of IRES across the gamut of river types worldwide. Global hydrological models are known to overestimate flow in arid climates[28], further complicating IRES mapping in these regions.

Finally, our model's ability to predict the natural prevalence of flow intermittence is affected by the impact of human activities on most gauged basins. Our study aims to depict the natural distribution of non-perennial watercourses by excluding those gauging stations from model training that were affected by flow regulation and/or whose flow intermittence class changed over the discharge record (see Methods). We also used naturalized estimates of discharge as predictor variables, which exclude anthropogenic water use in the form of abstractions or flow regulation. Nevertheless, disentangling the potential effects of contemporary land use, impoundments and human water abstractions on flow intermittence remains a research frontier[40]. We expect that continued improvements in global hydro-environmental datasets and hydrological models, combined with greater access to national hydrometric datasets, will be key to improve future IRES mapping efforts.

Understanding and managing IRES dynamics

Our global map of IRES may become a crucial tool for understanding and managing these long-undervalued ecosystems. High-resolution predictions of flow intermittence for all river reaches with MAF $\geq 0.1\ m^3\ s^{-1}$ can support spatially explicit studies down to the national scale, and our first-order extrapolation of the total prevalence of non-perennial rivers and streams by region and river basin can offer additional insights into the role of IRES at continental and global scales. Our results also provide an important baseline for the assessment of future changes in flow intermittence in river networks. Quantifying the variability of flow cessation in space and time is required to better understand the impact of climate change, water abstraction and flow regulation. IRES are not only becoming increasingly common but the flow regime of existing IRES can shift; for example, some intermittent rivers are becoming ephemeral, whereas others will turn perennial[41].

In this study we identified whether and where rivers and streams cease to flow, but further quantification of the spatiotemporal dynamics of flow occurrence across stream networks worldwide is required to determine when and for how long. Knowledge of the natural frequency, duration, and timing of flow cessation—the primary determinants of the functioning of IRES[2,3]—forms the basis of flow-alteration analyses that can inform strategies to mitigate the impacts of future changes[15]. In particular, tools for assessing environmental flows globally are needed to appraise freshwater planetary boundaries[42] and to define quantitative targets for the 2030 UN Sustainable Development Goals[43]. Yet current tools exclude arid and semi-arid regions[44], which are dominated by IRES and where alternative sources of water are scarce[5].

Rethinking the importance of IRES

Our findings call for a paradigm shift in river science and management. The foundational concepts of river hydrology, ecology and biogeochemistry have been developed from and for perennial waterways, and as a result, have all traditionally assumed year-round surface channel flow[9]. Here we show that this assumption is invalid for most rivers on Earth, which bolsters previous appeals for bringing together aquatic and terrestrial disciplines into river science[5,10].

Multiple conceptual models rely on the assumption that river discharge increases monotonically downstream from the headwaters to the mouth—for example, the River Continuum Concept[45], a theoretical pillar of river ecology. Moreover, current models define hydrological connectivity within river networks in binary terms, as either free-flowing or perpetually fragmented by barriers such as waterfalls and dams[46], but we show that temporary fragmentation by seasonal drying[47] is a widespread phenomenon on Earth. In hydrology, the parameterization and calibration of predictive models of runoff and discharge are usually based on average or peak flows (for example, for flood forecasting) rather than being calibrated to simulate low-flow quantities and timing, including flow cessation events, thus failing to reliably predict intermittence[20]. Up until now, global estimates of biodiversity have also overlooked IRES, which provide unique habitats for aquatic and terrestrial species[5,10]. Finally, recent research shows that omitting the role of non-perennial inland waters in carbon models may result in underestimating CO_2 emissions from inland waters by approximately 10%[4]; similar biases might undermine other global biogeochemical estimates, notably with respect to nitrogen cycling.

IRES have always been integral to human societies, whether culturally or as a source of food and water[5]. We estimate that for 52% of the world's population in 2020, the nearest river or stream is non-perennial (see Methods). The relationship between the seasonal hydrology of IRES and the ecosystem services they provide to society is a pressing area of research, particularly in regions where climate change is disrupting the water pulses to which people's livelihoods are tuned[48]. In many languages, multiple words exist to designate IRES and their mark on the landscape, highlighting the long history of inter-dependence between humans and seasonal freshwater systems[5]. However, the spiritual and cultural values that IRES provide, often to Indigenous peoples (for example, in Australia or in sub-Saharan Africa), remain to be acknowledged[5].

The past decade has witnessed several efforts to highlight both the values and ongoing degradation of IRES[6,8], yet current tools and policies still fall short of ensuring their biomonitoring and conservation[14,15]. A recognition of the prevalence and ecological importance of IRES by the scientific community may trigger efforts to adequately manage them and halt current attempts to exclude them from protective legislation[8]. As a stepping-stone, the dataset we present here intends to provide a baseline for identifying gaps in hydrological and biological monitoring efforts, to inform global biogeochemical upscaling and riverine species distribution models, and to decipher the links between hydrological patterns, culture and language. We hope it can ultimately assist in discerning the role of IRES in the Earth system to safeguard the integrity of river networks and the well-being of those who directly rely on these ecosystems for their livelihood and culture.

Online content

Any methods, additional references, Nature Research reporting summaries, source data, extended data, supplementary information, acknowledgements, peer review information; details of author contributions and competing interests; and statements of data and code availability are available at https://doi.org/10.1038/s41586-021-03565-5.

1. Larned, S. T., Datry, T., Arscott, D. B. & Tockner, K. Emerging concepts in temporary-river ecology. *Freshw. Biol.* **55**, 717–738 (2010).
2. Leigh, C. & Datry, T. Drying as a primary hydrological determinant of biodiversity in river systems: a broad-scale analysis. *Ecography* **40**, 487–499 (2017).
3. Datry, T. et al. A global analysis of terrestrial plant litter dynamics in non-perennial waterways. *Nat. Geosci.* **11**, 497–503 (2018).
4. Marcé, R. et al. Emissions from dry inland waters are a blind spot in the global carbon cycle. *Earth Sci. Rev.* **188**, 240–248 (2019).
5. Steward, A. L., von Schiller, D., Tockner, K., Marshall, J. C. & Bunn, S. E. When the river runs dry: human and ecological values of dry riverbeds. *Front. Ecol. Environ.* **10**, 202–209 (2012).
6. Acuña, V. et al. Why should we care about temporary waterways? *Science* **343**, 1080–1081 (2014).
7. Fritz, K., Cid, N. & Autrey, B. Governance, legislation, and protection of intermittent rivers and ephemeral streams. In *Intermittent Rivers and Ephemeral Streams: Ecology and Management* 477–507 (Academic Press, 2017); https://doi.org/10.1016/B978-0-12-803835-2.00019-X.
8. Sullivan, S. M. P., Rains, M. C., Rodewald, A. D., Buzbee, W. W. & Rosemond, A. D. Distorting science, putting water at risk. *Science* **369**, 766–768 (2020).
9. Allen, D. C. et al. River ecosystem conceptual models and non-perennial rivers: a critical review. *Wiley Interdiscip. Rev. Water* **7**, e1473 (2020).
10. Datry, T., Larned, S. T. & Tockner, K. Intermittent rivers: a challenge for freshwater ecology. *Bioscience* **64**, 229–235 (2014).
11. Ficklin, D. L., Abatzoglou, J. T., Robeson, S. M., Null, S. E. & Knouft, J. H. Natural and managed watersheds show similar responses to recent climate change. *Proc. Natl Acad. Sci. USA* **115**, 8553–8557 (2018).
12. Jaeger, K. L., Olden, J. D. & Pelland, N. A. Climate change poised to threaten hydrologic connectivity and endemic fishes in dryland streams. *Proc. Natl Acad. Sci. USA* **111**, 13894–13899 (2014).
13. Pumo, D., Caracciolo, D., Viola, F. & Noto, L. V. Climate change effects on the hydrological regime of small non-perennial river basins. *Sci. Total Environ.* **542**, 76–92 (2016).
14. Stubbington, R. et al. Biomonitoring of intermittent rivers and ephemeral streams in Europe: current practice and priorities to enhance ecological status assessments. *Sci. Total Environ.* **618**, 1096–1113 (2018).
15. Acuña, V. et al. Accounting for flow intermittency in environmental flows design. *J. Appl. Ecol.* **57**, 742–753 (2020).
16. Arthington, A. H. et al. The Brisbane Declaration and Global Action Agenda on Environmental Flows (2018). *Front. Environ. Sci.* **6**, 45 (2018).
17. Zimmer, M. A. et al. Zero or not? Causes and consequences of zero-flow stream gage readings. *Wiley Interdiscip. Rev. Water* **7**, e1436 (2020).
18. Beaufort, A., Lamouroux, N., Pella, H., Datry, T. & Sauquet, E. Extrapolating regional probability of drying of headwater streams using discrete observations and gauging networks. *Hydrol. Earth Syst. Sci.* **22**, 3033–3051 (2018).
19. Jaeger, K. L. & Olden, J. D. Electrical resistance sensor arrays as a means to quantify longitudinal connectivity of rivers. *River Res. Appl.* **28**, 1843–1852 (2012).
20. Yu, S. et al. Evaluating a landscape-scale daily water balance model to support spatially continuous representation of flow intermittency throughout stream networks. *Hydrol. Earth Syst. Sci.* **24**, 5279–5295 (2020).
21. Snelder, T. H. et al. Regionalization of patterns of flow intermittence from gauging station records. *Hydrol. Earth Syst. Sci.* **17**, 2685–2699 (2013).
22. Jaeger, K. L. et al. Probability of Streamflow Permanence Model (PROSPER): a spatially continuous model of annual streamflow permanence throughout the Pacific Northwest. *J. Hydrol. X* **2**, 100005 (2019).
23. Yu, S., Bond, N. R., Bunn, S. E. & Kennard, M. J. Development and application of predictive models of surface water extent to identify aquatic refuges in eastern Australian temporary stream networks. *Water Resour. Res.* **55**, 9639–9655 (2019).
24. Kennard, M. J. et al. Classification of natural flow regimes in Australia to support environmental flow management. *Freshw. Biol.* **55**, 171–193 (2010).
25. Lane, B. A., Dahlke, H. E., Pasternack, G. B. & Sandoval-Solis, S. Revealing the diversity of natural hydrologic regimes in California with relevance for environmental flows applications. *J. Am. Water Resour. Assoc.* **53**, 411–430 (2017).
26. Müller Schmied, H. et al. Sensitivity of simulated global-scale freshwater fluxes and storages to input data, hydrological model structure, human water use and calibration. *Hydrol. Earth Syst. Sci.* **18**, 3511–3538 (2014).
27. Linke, S. et al. Global hydro-environmental sub-basin and river reach characteristics at high spatial resolution. *Sci. Data* **6**, 283 (2019).
28. Tooth, S. Process, form and change in dryland rivers: a review of recent research. *Earth Sci. Rev.* **51**, 67–107 (2000).
29. Costigan, K. H., Jaeger, K. L., Goss, C. W., Fritz, K. M. & Goebel, P. C. Understanding controls on flow permanence in intermittent rivers to aid ecological research: integrating meteorology, geology and land cover. *Ecohydrology* **9**, 1141–1153 (2016).
30. Benstead, J. P. & Leigh, D. S. An expanded role for river networks. *Nat. Geosci.* **5**, 678–679 (2012).
31. Godsey, S. E. & Kirchner, J. W. Dynamic, discontinuous stream networks: hydrologically driven variations in active drainage density, flowing channels and stream order. *Hydrol. Processes* **28**, 5791–5803 (2014).
32. Metzger, M. J. et al. A high-resolution bioclimate map of the world: a unifying framework for global biodiversity research and monitoring. *Glob. Ecol. Biogeogr.* **22**, 630–638 (2013).
33. Tolonen, K. E. et al. Parallels and contrasts between intermittently freezing and drying streams: From individual adaptations to biodiversity variation. *Freshw. Biol.* **64**, 1679–1691 (2019).
34. Prancevic, J. P. & Kirchner, J. W. Topographic controls on the extension and retraction of flowing streams. *Geophys. Res. Lett.* **46**, 2084–2092 (2019).
35. FAO. *AQUAMAPS: Global Spatial Database on Water and Agriculture* (Food and Agriculture Organization of the United Nations, accessed 15 October 2020); https://data.apps.fao.org/aquamaps/
36. Schneider, A. et al. Global-scale river network extraction based on high-resolution topography and constrained by lithology, climate, slope, and observed drainage density. *Geophys. Res. Lett.* **44**, 2773–2781 (2017).
37. Raymond, P. A. et al. Global carbon dioxide emissions from inland waters. *Nature* **503**, 355–359 (2013); erratum **507**, 387 (2014).
38. Tramblay, Y. et al. Trends in flow intermittence for European rivers. *Hydrol. Sci. J.* **66**, 37–49 (2021).
39. Döll, P., Douville, H., Güntner, A., Müller Schmied, H. & Wada, Y. Modelling freshwater resources at the global scale: challenges and prospects. *Surv. Geophys.* **37**, 195–221 (2016).
40. Hammond, J. C. et al. Spatial patterns and drivers of nonperennial flow regimes in the contiguous United States. *Geophys. Res. Lett.* **48**, e2020GL090794 (2021).
41. Döll, P. & Schmied, H. M. How is the impact of climate change on river flow regimes related to the impact on mean annual runoff? A global-scale analysis. *Environ. Res. Lett.* **7**, 014037 (2012).
42. Gleeson, T. et al. The water planetary boundary: interrogation and revision. *One Earth* **2**, 223–234 (2020).
43. Dickens, C. et al. *Incorporating Environmental Flows into "Water Stress" Indicator 6.4.2: Guidelines for a Minimum Standard Method for Global Reporting* (FAO, 2019); http://www.fao.org/documents/card/en/c/ca3097en/
44. Sood, A. et al. *Global Environmental Flow Information for the Sustainable Development Goals*. IWMI Research Report 168 (International Water Management Institute, 2017); https://doi.org/10.5337/2017.201
45. Vannote, R. L., Minshall, G. W., Cummins, K. W., Sedell, J. R. & Cushing, C. E. The River Continuum Concept. *Can. J. Fish. Aquat. Sci.* **37**, 130–137 (1980).
46. Grill, G. et al. Mapping the world's free-flowing rivers. *Nature* **569**, 215–221 (2019); correction **572**, E9 (2019).
47. Stanley, E. H., Fisher, S. G. & Grimm, N. B. Ecosystem expansion and contraction in streams: desert streams vary in both space and time and fluctuate dramatically in size. *Bioscience* **47**, 427–435 (1997).
48. Datry, T. et al. Flow intermittence and ecosystem services in rivers of the Anthropocene. *J. Appl. Ecol.* **55**, 353–364 (2018).
49. Nembrini, S., König, I. R. & Wright, M. N. The revival of the Gini importance? *Bioinformatics* **34**, 3711–3718 (2018).

Methods

See Extended Data Fig. 7 for a summary of the data and methods used in this study.

Data

Global underpinning hydrography. We predicted the distribution of IRES for river reaches in the global RiverATLAS database[27]. RiverATLAS is a widely used representation of the global river network built on the hydrographic database HydroSHEDS[50,51]. Rivers are delineated on the basis of drainage direction and flow accumulation maps derived from elevation data at a pixel resolution of 3 arcseconds (~90 m at the equator) and subsequently upscaled to 15 arcseconds (~500 m at the equator). In this study, we only included river reaches with a modelled MAF ≥ 0.1 $m^3 s^{-1}$ and excluded: i) smaller streams (owing to increasing uncertainties in their geospatial location and flow estimates derived from global datasets and models; see also Methods section 'Hydro-environmental predictor variables' below); and ii) sections of river reaches within lakes (identified based on HydroLAKES polygons[52]). We define a 'river reach' as a cartographic—rather than a functional—unit, represented by the smallest spatial element of our global river network, that is, a line segment between two neighbouring confluences. We made predictions for 6,198,485 individual river reaches with an average length of 3.8 km, totalling 23.3 million kilometres of river network.

Reference intermittence data for model training and cross-validation. Two streamflow gauging station repositories were used as the source of training and cross-validation data for the split random forest (RF) model (Extended Data Figs. 7b, 8)—the World Meteorological Organization Global Runoff Data Centre (GRDC)[53] database ($n \approx 10{,}000$) and a complementary subset of the Global Streamflow Indices and Metadata archive (GSIM, $n \approx 31{,}000$), a compilation of twelve free-to-access national and international streamflow gauging station databases[54]. Whereas the GRDC offers daily river discharge values for most stations, GSIM only contains time series summary indices computed at the yearly, seasonal and monthly resolution (calculated from daily records whose open-access release is restricted for some of the compiled data sources)[55]. Therefore, we used the GRDC database as the core of our training/testing set and complemented it with a subset of streamflow gauging stations from GSIM. A GSIM station was included only if: i) it was not already part of the GRDC database; ii) it included auxiliary information on the drainage area of the monitored reach (for reliably associating it to RiverATLAS); iii) it had a drainage area <100 km^2 or else (that is, for gauges with a drainage area ≥100 km^2) it was located either iv) on an IRES or v) in a river basin that did not already contain a GRDC station (assessed based on level 5 sub-basins of the global BasinATLAS database[50], average sub-basin area = 2.9×10^4 km^2). We applied the described GSIM selection criteria to balance the relative amount of non-perennial versus perennial records, and the spatial distribution of stations in the model training dataset.

Each station in the combined dataset was geographically associated with a reach in the RiverATLAS stream network and every discharge time series was quality-checked through statistical and manual outlier detection (see Supplementary Information section II for details on these procedures). Non-perennial gauging stations were only included in the dataset if they were free of anomalous zero-flow values (for example, from instrument malfunction, gauge freezing, tidal flow reversal[17]). We also excluded stations whose streamflow was potentially dominated by reservoir outflow regulation (that is, with a degree of regulation >50%[27,56]) or whose discharge time series exhibited an alteration (see online research compendium at https://messamat.github.io/globalIRmap/ for an interactive visualization of processing information for every gauging station) as flow-regulating structures may change the flow class of a river either from perennial to non-perennial or vice-versa depending on their mode and rules of operation[57,58]. We further narrowed our selection by adding only gauging stations with a streamflow time series spanning at least 10 years—excluding years with more than 20 days of missing records for the calculation of this criterion and in subsequent analyses. Finally, we classified stations as non-perennial if their recorded discharge dropped to zero at least one day per year on average over the years of record, and as perennial otherwise. Stations with at least one zero-flow day per year on average (that is, non-perennial) but without a zero-flow day during 20 consecutive valid years of data (those with ≤20 missing days), anywhere in their record, were deemed either to have experienced a shift in flow intermittence class (regardless of the direction of the shift) or to have ceased to flow owing to exceptional conditions of drought and were also excluded. On the basis of these selection criteria, the training dataset contained data for 4,428 perennial river reaches and for 1,187 non-perennial reaches, with 41 and 34 years of daily streamflow data on average, respectively, across all continents (except Antarctica) (Extended Data Fig. 8).

The threshold used to define flow intermittence varies among studies, ranging from a single zero-flow day across the entire streamflow record[21,59] to at least five days per year on average[60]. Because zero-flow values in streamflow gauging records may be erroneous[17], other studies have used a flow percentile threshold value (for example, Q99 < 0.0283 $m^3 s^{-1}$ in the US Pacific Northwest)[22]. To test the sensitivity of altering our criterion (one zero-flow day per year on average) on the resulting number of non-perennial stations, we changed the threshold to one zero-flow month (30 consecutive or non-consecutive days) per year, which yielded a dataset with 4,735 perennial stations and 880 non-perennial stations, respectively. Given the substantial difference between these thresholds, we also produced model estimates for the latter definition (Extended Data Fig. 1b, c).

Although our training dataset of gauging stations encompasses a wide range of river types found on Earth, it is inherently limited by the global availability of hydrometric data (Extended Data Fig. 8). Most notably, rivers with MAF > 500 $m^3 s^{-1}$ are over-represented whereas those with MAF < 50 $m^3 s^{-1}$ are under-represented. In addition, few stations monitor rivers in extreme climates, whether cold or hot, dry or wet (for example, classes 1–4 and 16–18 for extremely cold and extremely hot climates, respectively; Extended Data Fig. 1a shows the extent of each climate stratum)[32]. Other under-represented river types include those with annual average snow cover extent >75% in their upstream drainage area and rivers with a shallow groundwater table or with >90% of karst outcrops across their upstream drainage area.

Hydro-environmental predictor variables. The primary source of predictor variables was the global RiverATLAS database, version 1.0, which is a subset of the broader HydroATLAS product[27]. RiverATLAS provides hydro-environmental information for all rivers of the world, both within their contributing local reach catchment and across the entire upstream drainage area of every reach (Extended Data Table 2). This information was derived by aggregating and reformatting original data from well established global digital maps, and by accumulating them along the drainage network from headwaters to ocean outlets[27].

RiverATLAS also includes estimates of long-term (1971–2000) naturalized (that is, without anthropogenic water use in the form of abstractions or impoundments) mean monthly and mean annual flow (MAF). These discharge estimates are derived through a geospatial downscaling procedure[50] based on the 0.5-degree resolution runoff and discharge layers provided by the global WaterGAP model (version 2.2 as of 2014)[26]. A validation of the downscaled discharge estimates against observations at the 2,131 GRDC gauging stations used in this study with ≥20 years of streamflow data from 1971 to 2000, representing rivers with MAF between 0.006 and 180,000 $m^3 s^{-1}$, confirmed good overall correlations for MAF (log–log least-square regression, $R^2 = 0.96$, with a symmetric mean absolute percentage error sMAPE of 30%; see Supplementary Table 1 for all validation results). The sMAPE increased from 5% for rivers with MAF ≥ 1,000 $m^3 s^{-1}$ to

20% for 10 $m^3 s^{-1} \leq MAF < 1{,}000\ m^3 s^{-1}$, and to 52% for MAF < 10 $m^3 s^{-1}$. Minimum monthly discharge was also found to be an effective proxy for Q90 (that is, the daily discharge exceeded 90% of days in the gauging record; $R^2 = 0.84$).

We complemented the RiverATLAS v1.0 data with three additional sets of variables. The first set of variables describes the inter-annual open surface water dynamics as determined by remote sensing imagery from 1999 to 2019[61]. In the original dataset, each 30-m-resolution pixel that has been covered by water sometime during this time period was assigned one of seven 'interannual dynamic classes' (for example, permanent water, stable seasonal, high-frequency changes) on the basis of a time series analysis of the annual percentage of open water in the pixel. We computed the percent coverage of each of these interannual dynamic classes relative to the total area of surface water within the contributing local catchment and across the entire upstream drainage area of every river reach.

Second, we replaced the soil and climate characteristics in RiverATLAS v1.0 with updated datasets. Specifically, we computed the average texture of the top 100 cm of soil based on version 2 of SoilGrids250m[62]. We also updated the climate variables with version 2 of WorldClim[63] (adding all bioclimatic variables to the existing set of variables) as well as the second version of the Global Aridity Index and Global Reference Evapotranspiration (Global-PET) datasets[64]. Finally, we updated the Climate Moisture Index (CMI), computed from the annual precipitation and potential evapotranspiration datasets provided by the WorldClim v2 and Global-PET v2 databases, respectively.

We derived a third set of variables by combining multiple variables already included in the model through algebraic operations. These metrics included the runoff coefficient (that is, the ratio of MAF and mean annual precipitation), specific discharge (that is, MAF per unit drainage area), and various temporal (for example, minimum annual/maximum annual discharge) and spatial (for example, mean elevation in local reach catchment/mean elevation in upstream drainage area) ratios.

The application of all described procedures yielded a total of 113 candidate predictor variables to be used in our statistical model development (Extended Data Table 2).

Machine learning models

We developed and used a split RF machine learning model to predict the flow intermittence class, as a probability response, of all river reaches globally, with 1 denoting a 100% predicted probability of being an IRES. RF models have already been successfully used to predict the distribution of IRES in Australia and France[21,65] and they have been shown to achieve high performance when compared to other approaches, including other machine learning models, logistic regression, and single decision trees[66,67]. Below, we briefly describe the model development and validation procedure conducted for our split RF model; see Supplementary Information section III for additional information.

Our final predictions are based on the probability RF algorithm developed by Malley et al.[68], a derivative of the standard RF algorithm for making probabilistic predictions of class membership, as included in the 'ranger' R package[69]. This algorithm was selected following a comparison[70,71] of several probability RF variants (namely, conditional inference forest[72,73] and a newly developed regression RF algorithm using maximally selected rank statistics[74]). To address known biases in RF models from class imbalance in the training data (more perennial than non-perennial gauging stations on large rivers)[22,75], we implemented random oversampling of non-perennial gauging stations[76].

For our split model approach, we trained and cross-validated two probability RF sub-models with slightly overlapping ranges in river size, one trained to predict the streamflow intermittence probability of small-to-medium rivers with MAF < 10 $m^3 s^{-1}$ and the other for medium-to-large rivers with MAF ≥ 1 $m^3 s^{-1}$. Within the overlapping range of 1–10 $m^3 s^{-1}$ MAF, the average probability was calculated to avoid abrupt transitions at a singular size threshold. This split approach performed better than a single model and was motivated by the distinct class imbalance in training gauging stations between large rivers (4.87:1 perennial to non-perennial ratio) versus small rivers (1.98:1 perennial to non-perennial ratio). With a single model, the use of a common oversampling factor for both size classes underpredicted the prevalence of IRES in large rivers (see Extended Data Table 3).

Model development and diagnostics

To optimize the predictive performance of the two sub-models, avoid overfitting, and obtain unbiased estimates of statistical uncertainty, we implemented a nested resampling framework for hyperparameter tuning and cross-validation[77], first for comparison across RF algorithm variants, and then for comparing model performance with and without predictor variable selection (see Supplementary Information section IV for a full description of the tuning and cross-validation procedure)[78,79]. Tuning was performed for 2–3 hyperparameters (depending on the RF algorithm) through random search with a termination criterion of 100 iterations. The inner (hyperparameter tuning) loop was composed of a fourfold cross-validation and the outer loop (for predictive performance assessment) involved a twice-repeated threefold cross-validation. Cross-validation strategies usually involve 2–10 folds[78], with a lower number of folds (as chosen here) yielding a more stringent evaluation of performance (that is, a pessimistic evaluation bias). The outer cross-validation procedure was repeated twice and the results were averaged to reduce the variance caused by randomly splitting the data into few folds[77]. A spatial cross-validation procedure based on k-means spatial clustering ($k = 40$, see Supplementary Fig. 3 for the distribution of clusters) was also used in the outer resampling loop to avoid overoptimistic error estimates that arise in cases of considerable spatial autocorrelation[80–83]. We chose to implement 40 spatial folds to strike a balance between two extremes. Fewer folds would risk evaluating the predictive ability of the model across areas so large that they may represent unique hydro-climatic conditions outside of the model's training set (for a given fold), therefore underestimating the model's performance. More folds would have inflated our estimate of model accuracy by relying on training sets too similar to the testing sets and would have made the computational requirements of cross-validation even greater.

All algorithms were compared using the same inner and outer sets of training and testing partitions. Hyperparameters were tuned to optimize the Balanced class ACCuracy (BACC) metric[84], which is equivalent to the raw accuracy (or one minus the misclassification rate) but with each sample weighted according to the inverse prevalence of its true class (large river model: 4.87 and 1.00 weights for the non-perennial and perennial classes, respectively; small river model: 1.98 and 1.00 for the non-perennial and perennial classes, respectively). To assess predictor variable importance, weighted averages of Actual Impurity Reduction (AIR, an unbiased version of Gini impurity)[49] and the associated p values (determined via 100 permutations, following ref. [85]) were computed for each outer resampling cross-validation fold and repetition, using the BACC of each resampling instance as weight.

Prior to final model training and evaluation, only predictors with a variable importance p value of <0.05 were retained, so that 92 and 82 variables were retained in the final small-river and large-river models, respectively. Variable selection was implemented to both increase model performance[86,87] and decrease model training time.

In addition to the BACC and the variable importance, several additional diagnostics were examined to determine the performance and characteristics of the RF model as follows:

(i) We assessed the classification accuracy (percentage of correctly classified gauges), the sensitivity (percentage of correctly classified IRES reaches, also known as true positive rate or recall), specificity (percentage of correctly classified perennial reaches, also known as true negative rate or selectivity), and precision (percentage of reaches

predicted to be IRES that are actually IRES) of the model for each streamflow size class (Extended Data Table 3), based on spatial and non-spatial cross-validations.

(ii) We examined the geographic, hydrological, and environmental distributions of the intermittence prediction residuals (IPRs) for each reference stream gauging station (Extended Data Fig. 2):

$$\text{IPR} = \text{predicted intermittence probability} - \text{observed intermittence class} \quad (1)$$

with observed intermittence class IR = {0: perennial, 1: non-perennial}. If |IPR| ≤ 0.5, the binary intermittence class of the reach associated with the gauging station was accurately predicted, with |IPR| values closer to 0.5 indicating greater uncertainty. If IPR > 0.5, the reach was predicted to be non-perennial when it was perennial. If IPR < −0.5, the reach was predicted to be perennial when it was non-perennial. We also examined the distribution of classification accuracy and bias (Fig. 3), as well as residual spatial autocorrelation (see Supplementary Information section IV.d), by river basin.

(iii) Partial dependence plots were generated for the 27 most important predictors using the 'edarf' package[88] (see Supplementary Fig. 5). These plots display estimates of the marginal relationship between each predictor variable and the model's predictions by holding the rest of the predictors at their respective mean values[89].

Assessing the global prevalence of IRES

After training the two final probability RF sub-models, the constructed prediction rules were used to estimate the probability of intermittence for each river reach included in the global river network (that is, with MAF ≥ 0.1 $m^3 s^{-1}$). All reaches with a resulting probability ≥0.5 were classified to be non-perennial (and perennial otherwise). This threshold was chosen following an analysis of model performance sensitivity to probability thresholds ranging from 0.25 to 0.75 for each RF sub-model which showed a balanced model performance at 0.5 (see Supplementary Information section IV.e). When adjusting the probability threshold between 0.45 and 0.55, the RF-predicted (that is, non-extrapolated) global prevalence of IRES varied from 36% to 48% (compared to 41% with a 0.5 threshold).

We then used the binary intermittence class predictions to compute the global prevalence of IRES by country, continent, climate zone, terrestrial biome, and major freshwater habitat type (Table 1 and Supplementary Data). Although gauging stations on reaches with MAF < 0.1 $m^3 s^{-1}$ were included in the training dataset, we did not produce global RF predictions of the probability of flow intermittence for individual reaches below this discharge threshold for two reasons. First, there existed only 59 gauges with MAF < 0.1 $m^3 s^{-1}$ and at least 10 valid years of data (including only 13 on perennial reaches), which was insufficient to confidently train a model and assess its uncertainty for this discharge size class. Second, there exists a discontinuity in RiverATLAS below 0.1 $m^3 s^{-1}$ whereby only those reaches with a drainage area ≥10 km^2 are included[27], leading to a varying discharge cut-off depending on a region's aridity. Nonetheless, bounding our RF predictions to 0.1 $m^3 s^{-1}$ enabled us to establish a robust estimate of the prevalence of flow intermittence in a range of discharge size classes which we then used for an extrapolation to smaller streams (see Methods section 'Extrapolating the global prevalence of IRES to smaller streams').

Estimating human population near IRES

To estimate the percentage of the global population living near an IRES, we first aggregated 2020 population count data from WorldPop[90]. We used constrained, rather than unconstrained, top-down WorldPop population estimates to avoid erroneous allocation of population to all land cells[90]. Population count estimates were aggregated from 3 arcsecond (~90 m at the equator) to 15 arcsecond pixels (~500 m, that is, the resolution of the hydrographic data underpinning the RiverATLAS river network). We associated the population within each larger pixel to the river reach in RiverATLAS (with MAF ≥ 0.1 $m^3 s^{-1}$) that was nearest to that pixel. Finally, we summed the population across all pixels in the world that were associated with a reach predicted to be non-perennial by our model.

Extrapolating the global prevalence of IRES to smaller streams

To create a first-order approximation of the global prevalence of IRES including even smaller streams, we extrapolated our model estimates to the next smaller streamflow size class range of [0.01, 0.1) $m^3 s^{-1}$. Although streams of this size class are rarely monitored or mapped globally, they are ecologically and environmentally critical[91]. For instance, at least 64% of rivers and streams in the USA (by length) show a MAF < 0.1 $m^3 s^{-1}$, and 25% show a MAF < 0.01 $m^3 s^{-1}$ (according to the US National Hydrography Dataset, NHDPlus, at medium resolution). We limited our extrapolation to one order of magnitude (that is, we did not include even smaller streams, with MAF < 0.01 $m^3 s^{-1}$, that still can form stream channels) as we expect uncertainties to continuously increase when moving further outside the range of our trained and tested RF model.

The prevalence of IRES for this stream size class was independently extrapolated for a total of 465 spatial sub-units representing all occurring intersections of 62 river basin regions (BasinATLAS[27] level 2 subdivisions, average surface area 2.2 × 10^6 km^2) and 18 climate zones (Global Environmental Stratification)[32]. For each basin–climate sub-unit, we first extrapolated the empirical cumulative distribution of total stream length (of all reaches with MAF ≥ 0.1 $m^3 s^{-1}$) down to 0.01 $m^3 s^{-1}$ MAF using a generalized additive model (GAM)[92]. We excluded reaches larger than the 95th percentile of MAF (that is, the largest rivers) within the sub-unit from model fitting to avoid common discontinuities at the high end of the empirical distribution that can affect the low end of the power-law-like trendline (see Supplementary Fig. 8a, c).

Second, we extrapolated the prevalence of flow intermittence (in percentage of stream length) down to 0.01 $m^3 s^{-1}$ MAF. In this case, we fitted a GAM for beta-distributed data—that is, with a (0, 1) range—to the prevalence of intermittence in each logarithmic MAF size bin of the sub-unit. MAF logarithmic size bins ($m^3 s^{-1}$) were defined as $[10^i, 10^{i+0.1})$ for every i in {−1, −0.9, −0.8, …, 5.3} for model fitting, and every i in {−2, −1.9, …, −1.1} for model extrapolation. See Supplementary Fig. 8b, d for illustrative examples of this approach. GAMs were used to conduct both extrapolations because this non-parametric, nonlinear approach does not require assumptions to be made regarding what distribution (for example, a power law[93]) the empirical cumulative distributions should follow. This is justifiable because the aim of the analysis was to make a pragmatic first-order approximation of IRES prevalence rather than to demonstrate the existence (or not) of a specific distribution.

Following the fitting of all GAM models, the length of IRES in each linear MAF size class between 0.01 $m^3 s^{-1}$ and 0.1 $m^3 s^{-1}$ was computed as the product of the extrapolated length of streams and the prevalence of intermittence in that size class. Finally, the total length of IRES in the extrapolated size classes was combined with the predictions from the split RF model to estimate the global prevalence of IRES as a percentage of the total global length of rivers and streams with MAF ≥ 0.01 $m^3 s^{-1}$.

We also produced an additional estimate with the assumption that, for each basin–climate sub-unit, the prevalence of IRES in streams with 0.01 ≤ MAF < 0.1 $m^3 s^{-1}$ was equal to the prevalence of IRES in streams with 0.1 ≤ MAF < 0.2 $m^3 s^{-1}$. Even with this conservative assumption, we estimate that 51% of all global rivers and streams with MAF ≥ 0.01 $m^3 s^{-1}$ are IRES. In contrast to the RF models, which estimate the probability of flow intermittence at the scale of individual river reaches, the GAM-based extrapolation provides aggregate estimates of IRES prevalence for basin–climate sub-units, which are best suited for global accounting studies.

Model comparisons

Comparisons with reported prevalence of flow intermittence at national scales. The most common source of information on the prevalence of flow intermittence across large regions are national hydrographic datasets, derived mainly from paper topographic maps in which non-perennial watercourses are usually depicted by dashed lines. We compared our model estimates of the percentage of stream length that is non-perennial with this type of hydrographic data for four countries covering a wide range of environmental, geological, and climatic conditions: the contiguous USA, Australia, Brazil, and Argentina (Extended Data Figs. 3, 4; for data sources see Extended Data Fig. 7b). In addition, we compared our results in mainland France with predictions of a national model[21].

It should be noted that we do not consider these comparisons to be an accuracy assessment of our model outputs, owing to the inherent yet unknown uncertainties in the national hydrographic datasets. Although the national maps represent the most comprehensive records of presumed intermittence, most are characterized by high levels of inconsistency among regions and cartographers, even for a fixed map scale (for example, 1:24,000), in both stream density and flow intermittence assessment[94,95]. For instance, streamflow intermittence classifications contained in the US National Hydrography Dataset (NHDPlus, which was used in this study), based on one-time field surveys typically conducted in the mid-to-late 1900s, have been shown to exhibit misclassification rates as high as 50% compared to independent field surveys[94,95]. Hafen et al.[96] report only an 80–81% agreement between ground-based streamflow field observations from the US Pacific Northwest and the NHDPlus classifications. Furthermore, in the Brazilian dataset and the NHDPlus, neighbouring topographic map sheets differ in whether flow intermittence was mapped, leading to artefactual hard edges between regions in terms of the prevalence of intermittence[97] (for example, Extended Data Fig. 4). Despite these limitations, map-based national hydrographic datasets remain the reference used by most government agencies and institutions in determining the extent and flow intermittence of river networks, and thus provide a useful benchmark for comparing the output of our model.

A custom processing workflow was developed to format each of the four national river network datasets to ensure comparability with our model predictions. This involved filtering each source dataset to keep only river and stream channels (for example, excluding lake shorelines and marine coastlines), excluding reaches in the source data that do not correspond with the streamflow threshold applied for the mapped rivers in this study (MAF $\geq 0.1\ m^3\ s^{-1}$) and excluding artificial channels (for example, canals and ditches). For a full description of the formatting workflow, see Supplementary Information section VI.a. Following this formatting process, we compared the percentage of river network length that was categorized as IRES in each of the source datasets to our model results for the same region (Extended Data Fig. 5). We could not perform this quantitative comparison for Brazil and Argentina because there was no measure of river size in these datasets. Lastly, we visually assessed whether spatial patterns of intermittence were similar between the source datasets and our model results. Aside from Argentina, we were unable to compare our predictions to hydrographic maps in countries where sparse hydrometric networks result in higher modelling uncertainties, owing to the unavailability of hydrographic data in these regions.

Comparisons with local on-the-ground visual observations. Datasets of on-the-ground visual observations of flow presence or absence (flow state) by trained individuals provide some of the most reliable records of flow intermittence[22,98,99]. We compared our predictions of intermittence to datasets of this type for two regions: the US Pacific Northwest and mainland France (Extended Data Fig. 6; see Supplementary Information section VI.b for additional details). We did not use these observations directly for the training of the RF sub-models as we could not apply the same criterion to define 'intermittence' as for gauging stations (that is, at least one day per year of flow cessation, on average, across the entire record) and their inclusion would have represented a strong regional bias. These datasets instead enabled an independent comparison of the model predictions for smaller rivers and streams (here mostly $<1\ m^3\ s^{-1}$), which are poorly represented in the global hydrometric network.

For the US Pacific Northwest, we used 5,372 observations across 3,725 reaches (3,547 perennial, 178 non-perennial) from a larger dataset of 24,316 stream observations[100] that occurred from 1 July to 1 October, between 1977 and 2016. The source dataset is a compilation of 11 smaller datasets from independent projects that include aquatic species habitat surveys, wet/dry stream channel mapping, beneficial use reconnaissance surveys, or were collected specifically for the PROSPER intermittent river mapping project[22,100]. Streamflow observations included one-time surveys and repeat surveys extending over several years, as well as discrete locations or continuous sections of a stream channel reach. On the basis of the approach used by Jaeger et al.[22], we considered that a river section was perennial only if all observations (1 July–1 October) reported the presence of water. Despite this strict criterion, this dataset may underestimate the prevalence of intermittence since most sites were only observed 1–3 times and the probability that flow cessation was observed at a given reach increased with the number of observations (logistic regression, $n = 9{,}850$, $p < 0.001$, see Supplementary Information section VI.b for details).

For France, we used 124,112 observations across 2,297 reaches (878 perennial, 1,419 non-perennial) from a larger set of approximately 3,300 sites uniformly distributed across France from the national river drying observatory (ONDE) network[101]. The ONDE network provides a stable set of sites on river and stream reaches of Strahler orders under five which, since 2012, have been inspected by agency employees from the French Office for Biodiversity (OFB) at least monthly between May and September. We considered an observation to reflect flow intermittence if it was classified as either 'with no visible flow' or 'dried out' (as opposed to 'with visible flow'). In case of multiple observations on one reach, we considered the reach to be non-perennial if a single observation of flow cessation existed.

All flow state observations were linked to the RiverATLAS stream network through custom semi-automated procedures designed for each dataset, using the proximity between the point observations and the reach locations in RiverATLAS, as well as associated information from local river network datasets and ancillary attribute data provided for each location (for example, drainage area, site name; see Supplementary Information section VI.b for details). Following data formatting and harmonization, we assessed the degree of agreement at the river reach level between the binary intermittence class predicted by our model and that reported by the two datasets of visual observations.

Data availability

The global river network dataset and the associated attribute information for every river reach—that is, the hydro-environmental attributes, predicted probability of intermittence and associated binary class—as well as the main results of the study are available at https://doi.org/10.6084/m9.figshare.14633022. The dataset can be used together with the published source code (see 'Code availability') to recalculate the main study results with updated data and parameters. The streamflow time series from the Global Runoff Data Centre are available in summarized format. The daily records are not available in the data repository owing to licensing issues but are freely available upon written request through https://www.bafg.de/GRDC/EN/Home/homepage_node.html. Original data that supported the study are freely available and their sources are summarized in Extended Data Fig. 7b. Source data are provided with this paper.

Code availability

The source code and results of this research are available under the GNU General Public License v3.0 at https://messamat.github.io/globalIRmap/.

50. Lehner, B. & Grill, G. Global river hydrography and network routing: baseline data and new approaches to study the world's large river systems. *Hydrol. Processes* **27**, 2171–2186 (2013).
51. Lehner, B., Verdin, K. & Jarvis, A. New global hydrography derived from spaceborne elevation data. *Eos* **89**, 93–94 (2008).
52. Messager, M. L., Lehner, B., Grill, G., Nedeva, I. & Schmitt, O. Estimating the volume and age of water stored in global lakes using a geo-statistical approach. *Nat. Commun.* **7**, 13603 (2016).
53. Global Runoff Data Centre. *In-situ river discharge data* (World Meteorological Organization, accessed 15 May 2015); https://portal.grdc.bafg.de/applications/public.html?publicuser=PublicUser#dataDownload/Home
54. Do, H. X., Gudmundsson, L., Leonard, M. & Westra, S. The Global Streamflow Indices and Metadata Archive (GSIM) – Part 1: The production of a daily streamflow archive and metadata. *Earth Syst. Sci. Data* **10**, 765–785 (2018).
55. Gudmundsson, L., Do, H. X., Leonard, M. & Westra, S. The Global Streamflow Indices and Metadata Archive (GSIM) – Part 2: Quality control, time-series indices and homogeneity assessment. *Earth Syst. Sci. Data* **10**, 787–804 (2018).
56. Lehner, B. et al. High-resolution mapping of the world's reservoirs and dams for sustainable river-flow management. *Front. Ecol. Environ*. **9**, 494–502 (2011).
57. Mackay, S. J., Arthington, A. H. & James, C. S. Classification and comparison of natural and altered flow regimes to support an Australian trial of the Ecological Limits of Hydrologic Alteration framework. *Ecohydrology* **7**, 1485–1507 (2014).
58. Zhang, Y., Zhai, X., Shao, Q. & Yan, Z. Assessing temporal and spatial alterations of flow regimes in the regulated Huai River Basin, China. *J. Hydrol*. **529**, 384–397 (2015).
59. Reynolds, L. V., Shafroth, P. B. & LeRoy Poff, N. Modeled intermittency risk for small streams in the Upper Colorado River Basin under climate change. *J. Hydrol.* **523**, 768–780 (2015).
60. Costigan, K. H. et al. Flow regimes in intermittent rivers and ephemeral streams. In *Intermittent Rivers and Ephemeral Streams: Ecology and Management* 51–78 (Academic Press, 2017); https://doi.org/10.1016/B978-0-12-803835-2.00003-6
61. Pickens, A. H. et al. Mapping and sampling to characterize global inland water dynamics from 1999 to 2018 with full Landsat time-series. *Remote Sens. Environ*. **243**, 111792 (2020).
62. Hengl, T. et al. SoilGrids250m: Global gridded soil information based on machine learning. *PLoS ONE* **12**, e0169748 (2017).
63. Fick, S. E. & Hijmans, R. J. WorldClim 2: new 1-km spatial resolution climate surfaces for global land areas. *Int. J. Climatol*. **37**, 4302–4315 (2017).
64. Trabucco, A. & Zomer, R. Global Aridity Index and Potential Evapotranspiration (ET0) Climate Database v2. figshare https://doi.org/10.6084/m9.figshare.7504448.v3 (2018).
65. Bond, N. R. & Kennard, M. J. Prediction of hydrologic characteristics for ungauged catchments to support hydroecological modeling. *Water Resour. Res*. **53**, 8781–8794 (2017).
66. Kotsiantis, S. B., Zaharakis, I. D. & Pintelas, P. E. Machine learning: a review of classification and combining techniques. *Artif. Intell. Rev*. **26**, 159–190 (2006).
67. Wainer, J. Comparison of 14 different families of classification algorithms on 115 binary datasets. Preprint at https://arxiv.org/abs/1606.00930 (2016).
68. Malley, J. D., Kruppa, J., Dasgupta, A., Malley, K. G. & Ziegler, A. Probability machines. *Methods Inf. Med*. **51**, 74–81 (2012).
69. Wright, M. N. & Ziegler, A. ranger: a fast implementation of random forests for high dimensional data in C++ and R. *J. Stat. Softw*. **77**, https://doi.org/10.18637/jss.v077.i01 (2017).
70. Lang, M. et al. mlr3: a modern object-oriented machine learning framework in R. *J. Open Source Softw*. **4**, 1903 (2019).
71. Landau, W. M. The drake R package: a pipeline toolkit for reproducibility and high-performance computing. *J. Open Source Softw*. **3**, 550 (2018).
72. Hothorn, T., Hornik, K. & Zeileis, A. Unbiased recursive partitioning: a conditional inference framework. *J. Comput. Graph. Stat*. **15**, 651–674 (2006).
73. Hothorn, T. & Zeileis, A. Partykit: a modular toolkit for recursive partytioning in R. *J. Mach. Learn. Res*. **16**, 3905–3909 (2015).
74. Wright, M. N., Dankowski, T. & Ziegler, A. Unbiased split variable selection for random survival forests using maximally selected rank statistics. *Stat. Med*. **36**, 1272–1284 (2017).
75. Zhang, G. & Lu, Y. Bias-corrected random forests in regression. *J. Appl. Stat*. **39**, 151–160 (2012).
76. Japkowicz, N. & Stephen, S. The class imbalance problem: a systematic study. *Intell. Data Anal*. **6**, 429–449 (2002).
77. Bischl, B., Mersmann, O., Trautmann, H. & Weihs, C. Resampling methods for meta-model validation with recommendations for evolutionary computation. *Evol. Comput*. **20**, 249–275 (2012).
78. Probst, P., Wright, M. N. & Boulesteix, A. L. Hyperparameters and tuning strategies for random forest. *Wiley Interdiscip. Rev. Data Min. Knowl. Discov*. **9**, e1301 (2019).
79. Probst, P. & Boulesteix, A. L. To tune or not to tune the number of trees in random forest. *J. Mach. Learn. Res*. **18**, 1–8 (2018).
80. Schratz, P., Muenchow, J., Iturritxa, E., Richter, J. & Brenning, A. Hyperparameter tuning and performance assessment of statistical and machine-learning algorithms using spatial data. *Ecol. Modell*. **406**, 109–120 (2019).
81. Brenning, A. Spatial cross-validation and bootstrap for the assessment of prediction rules in remote sensing: the R package sperrorest. In *2012 IEEE Int. Geoscience and Remote Sensing Symp. (IGARSS)* 5372–5375 (2012); https://doi.org/10.1109/IGARSS.2012.6352393
82. Meyer, H., Reudenbach, C., Hengl, T., Katurji, M. & Nauss, T. Improving performance of spatio-temporal machine learning models using forward feature selection and target-oriented validation. *Environ. Model. Softw*. **101**, 1–9 (2018).
83. Meyer, H., Reudenbach, C., Wöllauer, S. & Nauss, T. Importance of spatial predictor variable selection in machine learning applications – moving from data reproduction to spatial prediction. *Ecol. Modell*. **411**, 108815 (2019).
84. Brodersen, K. H., Ong, C. S., Stephan, K. E. & Buhmann, J. M. The balanced accuracy and its posterior distribution. In *Proc. Int. Conf. Pattern Recognition* 3121–3124 (2010); https://doi.org/10.1109/ICPR.2010.764
85. Altmann, A., Toloşi, L., Sander, O. & Lengauer, T. Permutation importance: a corrected feature importance measure. *Bioinformatics* **26**, 1340–1347 (2010).
86. Amaratunga, D., Cabrera, J. & Lee, Y.-S. Enriched random forests. *Bioinformatics* **24**, 2010–2014 (2008).
87. Evans, J. S., Murphy, M. A., Holden, Z. A. & Cushman, S. A. Modeling species distribution and change using random forest. In *Predictive Species and Habitat Modeling in Landscape Ecology: Concepts and Applications* 139–159 (Springer, 2011); https://doi.org/10.1007/978-1-4419-7390-0_8
88. Jones, Z. M. & Linder, F. J. edarf: Exploratory Data Analysis using Random Forests. *J. Open Source Softw*. **1**, 92 (2016).
89. Friedman, J. H. Greedy function approximation: a gradient boosting machine. *Ann. Stat*. **29**, 1189–1232 (2001).
90. Bondarenko, M., Kerr, D., Sorichetta, A. & Tatem, A. J. *Census/projection-disaggregated gridded population datasets for 189 countries in 2020 using Built-Settlement Growth Model (BSGM) outputs* (WorldPop, University of Southampton, accessed 26 November 2020); https://doi.org/10.5258/SOTON/WP00684
91. Colvin, S. A. R. et al. Headwater streams and wetlands are critical for sustaining fish, fisheries, and ecosystem services. *Fisheries* **44**, 73–91 (2019).
92. Hastie, T., Tibshirani, R. & Friedman, J. *The Elements of Statistical Learning: Data Mining, Inference, and Prediction* (Springer Science & Business Media, 2009).
93. Clauset, A., Shalizi, C. R. & Newman, M. E. J. Power-law distributions in empirical data. *SIAM Rev*. **51**, 661–703 (2009).
94. Fritz, K. M. et al. Comparing the extent and permanence of headwater streams from two field surveys to values from hydrographic databases and maps. *J. Am. Water Resour. Assoc*. **49**, 867–882 (2013).
95. Stoddard, J. L. et al. *Environmental Monitoring and Assessment Program (EMAP): Western Streams and Rivers Statistical Summary*. Report no. EPA/620/R-05/006 (NTIS PB2007-102088) (US Environmental Protection Agency, 2005).
96. Hafen, K. C., Blasch, K. W., Rea, A., Sando, R. & Gessler, P. E. The influence of climate variability on the accuracy of NHD perennial and nonperennial stream classifications. *J. Am. Water Resour. Assoc*. **56**, 903–916 (2020).
97. Colson, T., Gregory, J., Dorney, J. & Russell, P. Topographic and soil maps do not accurately depict headwater stream networks. *Natl Wetlands Newsl*. **30**, 25–28 (2008).
98. Allen, D. C. et al. Citizen scientists document long-term streamflow declines in intermittent rivers of the desert southwest, USA. *Freshw. Sci*. **38**, 244–256 (2019).
99. Datry, T., Pella, H., Leigh, C., Bonada, N. & Hugueny, B. A landscape approach to advance intermittent river ecology. *Freshw. Biol*. **61**, 1200–1213 (2016).
100. McShane, R. R., Sando, R. & Hockman-Wert, D. P. Streamflow observation points in the Pacific Northwest, 1977–2016. U.S. Geological Survey data release https://doi.org/10.5066/F7BV7FSP (2017).
101. *Observatoire National des étiages (ONDE)* (French Office for Biodiversity (OFC), accessed 21 June 2020); https://onde.eaufrance.fr/content/t%C3%A9l%C3%A9charger-les-donn%C3%A9es-des-campagnes-par-ann%C3%A9e
102. *Aguas Continentales de Argentina* (Argentinian National Geographic Institute (IGN), accessed 11 June 2020); https://www.ign.gob.ar/NuestrasActividades/InformacionGeoespacial/CapasSIG
103. *Australian Hydrological Geospatial Fabric (Geofabric, v. 3.2)* (Australian Bureau of Meteorology (BOM), accessed 11 June 2020); ftp://ftp.bom.gov.au/anon/home/geofabric/Geofabric_Metadata_GDB_V3_2.zip
104. *Base Cartográfica Continua do Brasil (BC250, 2019 version)* (Brazilian Institute of Geography and Statistics (IBGE); accessed 11 June 2020); https://geoftp.ibge.gov.br/cartas_e_mapas/bases_cartograficas_continuas/bc250/versao2019/
105. *National Hydrography Dataset Plus (NHDPlus, medium resolution, v.2)* (US Geological Survey, accessed 11 June 2020); https://www.epa.gov/waterdata/get-nhdplus-national-hydrography-dataset-plus-data
106. Busch, M. H. et al. What's in a name? Patterns, trends, and suggestions for defining non-perennial rivers and streams. *Water* **12**, 1980 (2020).
107. Datry, T. et al. Science and management of intermittent rivers and ephemeral streams (SMIRES). *Res. Ideas Outcomes* **3**, e21774 (2017).
108. Trabucco, A. & Zomer, R. J. Global high-resolution soil–water balance. https://doi.org/10.6084/m9.figshare.7707605.v3 (2010).
109. Hall, D. K. & Riggs, G. A. *MODIS/Aqua Snow Cover Daily L3 Global 500m SIN Grid, Version 6. [2002–2015]* (NASA National Snow and Ice Data Center Distributed Active Archive Center, accessed 15 February 2017); https://doi.org/10.5067/MODIS/MYD10A1.006
110. Fan, Y., Li, H. & Miguez-Macho, G. Global patterns of groundwater table depth. *Science* **339**, 940–943 (2013).
111. Fluet-Chouinard, E., Lehner, B., Rebelo, L.-M., Papa, F. & Hamilton, S. K. Development of a global inundation map at high spatial resolution from topographic downscaling of coarse-scale remote sensing data. *Remote Sens. Environ*. **158**, 348–361 (2015).
112. Döll, P., Kaspar, F. & Lehner, B. A global hydrological model for deriving water availability indicators: model tuning and validation. *J. Hydrol*. **270**, 105–134 (2003).
113. Bartholomé, E. & Belward, A. S. GLC2000: a new approach to global land cover mapping from Earth observation data. *Int. J. Remote Sens*. **26**, 1959–1977 (2005).
114. GLIMS and National Snow and Ice Data Center. *GLIMS Glacier Database V1* (2012); https://doi.org/10.7265/N5V98602
115. Gruber, S. Derivation and analysis of a high-resolution estimate of global permafrost zonation. *Cryosphere* **6**, 221–233 (2012).
116. Ramankutty, N. & Foley, J. A. Estimating historical changes in global land cover: croplands from 1700 to 1992. *Glob. Biogeochem. Cycles* **13**, 997–1027 (1999).
117. Lehner, B. & Döll, P. Development and validation of a global database of lakes, reservoirs and wetlands. *J. Hydrol*. **296**, 1–22 (2004).

118. Robinson, N., Regetz, J. & Guralnick, R. P. EarthEnv-DEM90: a nearly-global, void-free, multi-scale smoothed, 90m digital elevation model from fused ASTER and SRTM data. *ISPRS J. Photogramm. Remote Sens.* **87**, 57–67 (2014).
119. Williams, P. W. & Ford, D. C. Global distribution of carbonate rocks. *Z. Geomorphol. Suppl.* **147**, 1–2 (2006).
120. Hartmann, J. & Moosdorf, N. The new global lithological map database GLiM: a representation of rock properties at the Earth surface. *Geochem. Geophys. Geosyst.* **13**, Q12004 (2012).

Acknowledgements We thank T. Elrick and the Geographic Information Centre at McGill University for providing us with high-performance computing resources, and the Global Runoff Data Centre (GRDC) for providing us with global streamflow gauging data. Funding for this study was provided in part by the Natural Sciences and Engineering Research Council of Canada (B.L., C.C., C.W., M.L.M., NSERC Discovery grants RGPIN/341992-2013 and RGPIN/04541-2019); McGill University (M.L.M., Tomlinson Fellowship), Montreal, Quebec, Canada; H_2O'Lyon Doctoral School (M.L.M., Doctoral Fellowship, ANR-17-EURE-0018), Lyon, France; T.D., N.L., H.P. and T.T. were supported by the DRYvER project (http://www.dryver.eu/), which has received funding from the European Union's Horizon 2020 research and innovation programme under grant agreement no. 869226.

Author contributions CRediT (Contributor Roles Taxonomy): conceptualization—T.D., B.L., K.T., M.L.M.; methodology—M.L.M., B.L., T.S., C.C., N.L.; data curation—M.L.M., B.L., C.C., C.W., T.S., H.P.; software, validation, visualization—M.L.M.; formal analysis—M.L.M., C.C.; writing original draft—M.L.M., T.D., B.L.; writing, review and editing—all authors; project administration and supervision—M.L.M., B.L., T.D.; funding acquisition—B.L., T.D., M.L.M.

Competing interests The authors declare no competing interests.

Additional information

Supplementary information The online version contains supplementary material available at https://doi.org/10.1038/s41586-021-03565-5.

Correspondence and requests for materials should be addressed to M.L.M., B.L. or T.D.

Peer review information *Nature* thanks Kristin Jaeger, Georgia Papacharalampous and the other, anonymous, reviewer(s) for their contribution to the peer review of this work. Peer reviewer reports are available.

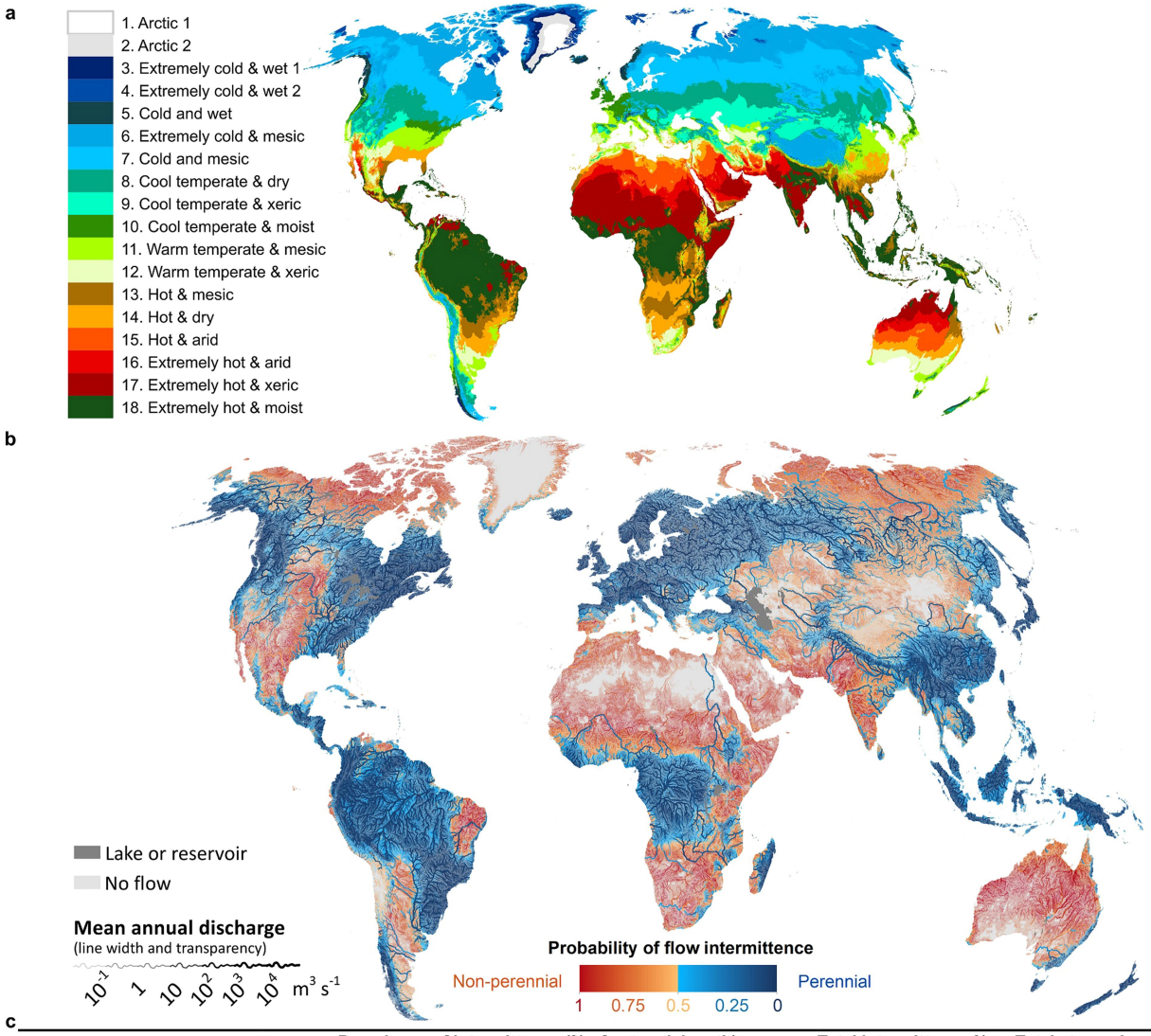

c

Climate zone	Prevalence of intermittence (% of network length) by streamflow size class ($m^3 s^{-1}$)							Total intermittence % length	Total stream length 10^3 km
	extrapolated	mapped						including | (excluding) extrapolated stream class	
	[10^{-2},10^{-1})	[10^{-1},1)	[1,10)	[10,10^2)	[10^2,10^3)	[10^3,10^4)	≥ 10^4		
Extremely hot and arid	*100*	100	100	97	39	0	-	99 | (98)	1,032 | (249)
Hot and arid	*100*	100	100	96	47	0	-	99 | (98)	990 | (238)
Arctic 1	*100*	100	100	100	-	-	-	100 | (100)	11 | (6)
Warm temperate and xeric	*99*	95	84	49	8	0	0	95 | (87)	1,351 | (444)
Extremely cold and wet 2	*99*	95	87	42	18	-	-	97 | (92)	766 | (243)
Extremely hot and xeric	*98*	88	89	86	31	0	0	94 | (85)	4,551 | (1,605)
Arctic 2	*100*	99	98	22	-	-	-	99 | (99)	98 | (41)
Cool temperate and xeric	*86*	74	54	19	0	0	-	78 | (62)	1,709 | (552)
Extremely cold and mesic	*87*	64	45	34	29	23	0	75 | (57)	8,083 | (3,051)
Extremely cold and wet 1	*92*	75	62	9	0	-	-	82 | (72)	227 | (109)
Cold and mesic	*56*	32	20	5	3	0	0	45 | (26)	8,189 | (3,084)
Warm temperate and mesic	*79*	30	18	7	0	0	0	54 | (24)	3,582 | (1,646)
Hot and dry	*71*	41	28	18	4	0	0	56 | (35)	4,054 | (1,683)
Cool temperate and dry	*55*	36	22	7	0	0	0	47 | (29)	4,087 | (1,325)
Hot and mesic	*68*	26	17	19	4	0	0	47 | (22)	4,452 | (2,023)
Extremely hot and moist	*38*	14	14	17	2	0	0	30 | (14)	19,117 | (6,002)
Cool temperate and moist	*31*	7	3	0	0	0	-	16 | (5)	1,164 | (691)
Cold and wet	*7*	2	0	0	0	0	-	2 | (1)	493 | (299)
World	*63*	**41**	**28**	**23**	**7**	**1**	**0**	**53 | (35)**	**63,956 | (23,291)**

Extended Data Fig. 1 | See next page for caption.

Extended Data Fig. 1 | Global prevalence of IRES with at least one zero-flow month per year on average. a, Distribution of global climate zones used in this study. Data provided by Global Environmental Stratification (GEnS)[32]. **b**, Predicted probability of river flow intermittence, defined as at least one zero-flow month (30 days) per year on average, across the global river and stream network[27]. The median probability threshold of 0.5 was used to determine the binary flow intermittence class for each reach. **c**, Global prevalence of IRES with at least one zero-flow month (30 days) per year on average, across climate zones and streamflow size classes (based on long-term average naturalized discharge). Note that in regions with sparse training data, the model results can differ substantially from the results shown in Table 1, as the underlying random forest and extrapolation models were developed independently. No stations were available in climate zones Arctic 1 and Arctic 2, and few stations were available in 'Extremely cold and wet' (1 and 2) and in 'Extremely hot and arid' climates (together representing 3% of global river and stream length). Rows are sorted in the same order as in Table 1, and the same footnotes as in Table 1 apply. Mapping software: ArcMap (ESRI).

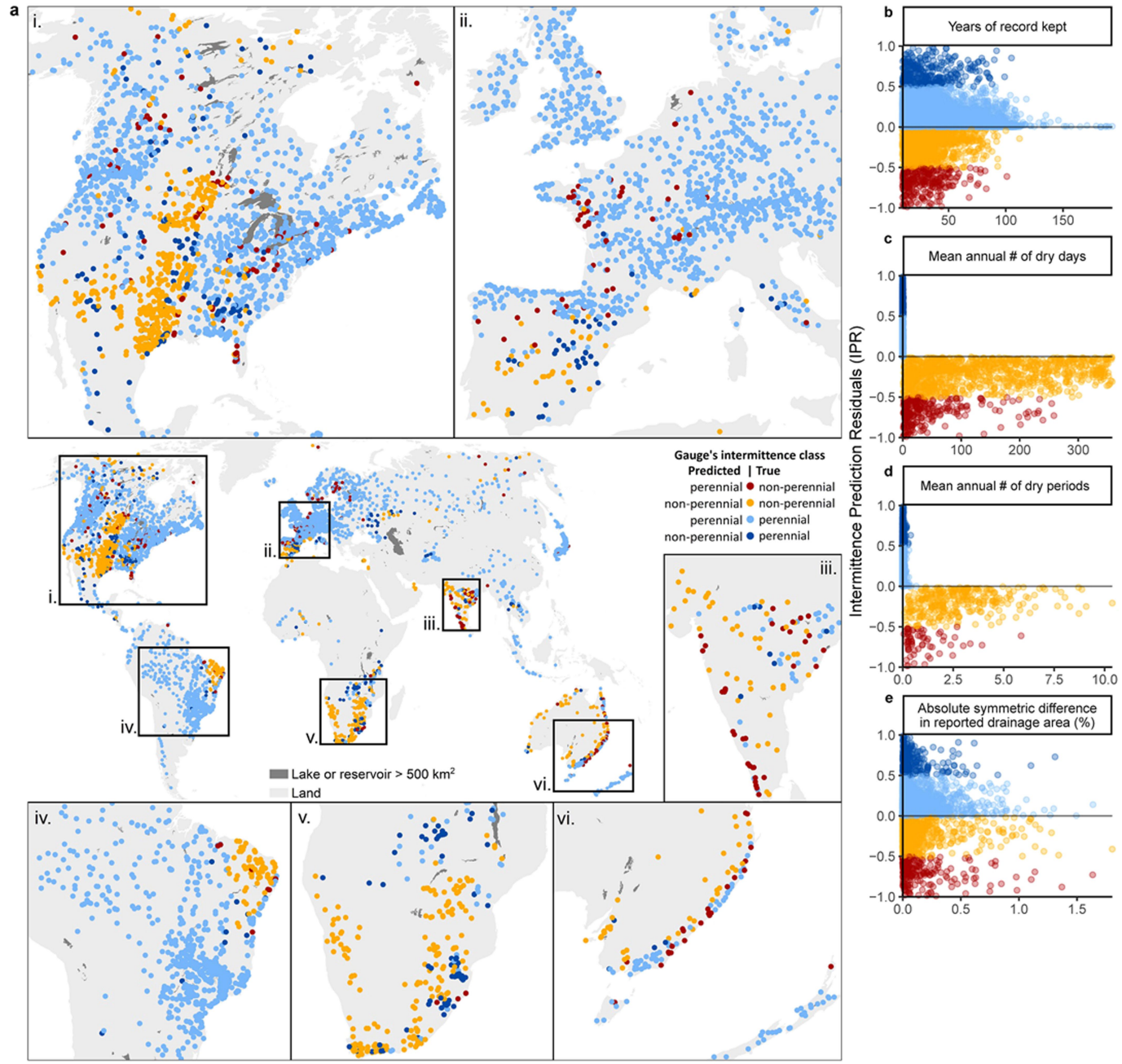

Extended Data Fig. 2 | Distribution of cross-validation results. a, Maps of spatially cross-validated predictive accuracy of flow intermittence for streamflow gauging stations. See Supplementary Fig. 3 for the distribution of spatial cross-validation folds and details on the cross-validation procedure. The classification errors shown here are not necessarily present in the final predictions but illustrate the ability of the model to predict the flow intermittence class for each region if that region was excluded from the training set. For instance, it shows that the model would be unable to predict the presence of IRES in western France and northern Spain (inset ii, dark red dots), or in western India (inset iii) without training stations in these regions. **b**–**e**, Intermittence prediction residuals versus gauging station characteristics and environmental variables. The mean intermittence prediction residual (IPR) is the difference between the average predicted probability of flow intermittence (across three cross-validation folds and two repetitions) and the observed flow intermittence of the gauging station (1 = non-perennial, 0 = perennial). Overall, prediction errors and uncertainties decrease with an increase in the number of recorded years by gauging stations as well as the drainage area and the degree of flow intermittence (average annual number of zero-flow days and flow cessation events) of the corresponding reaches. Mapping software: ArcMap (ESRI).

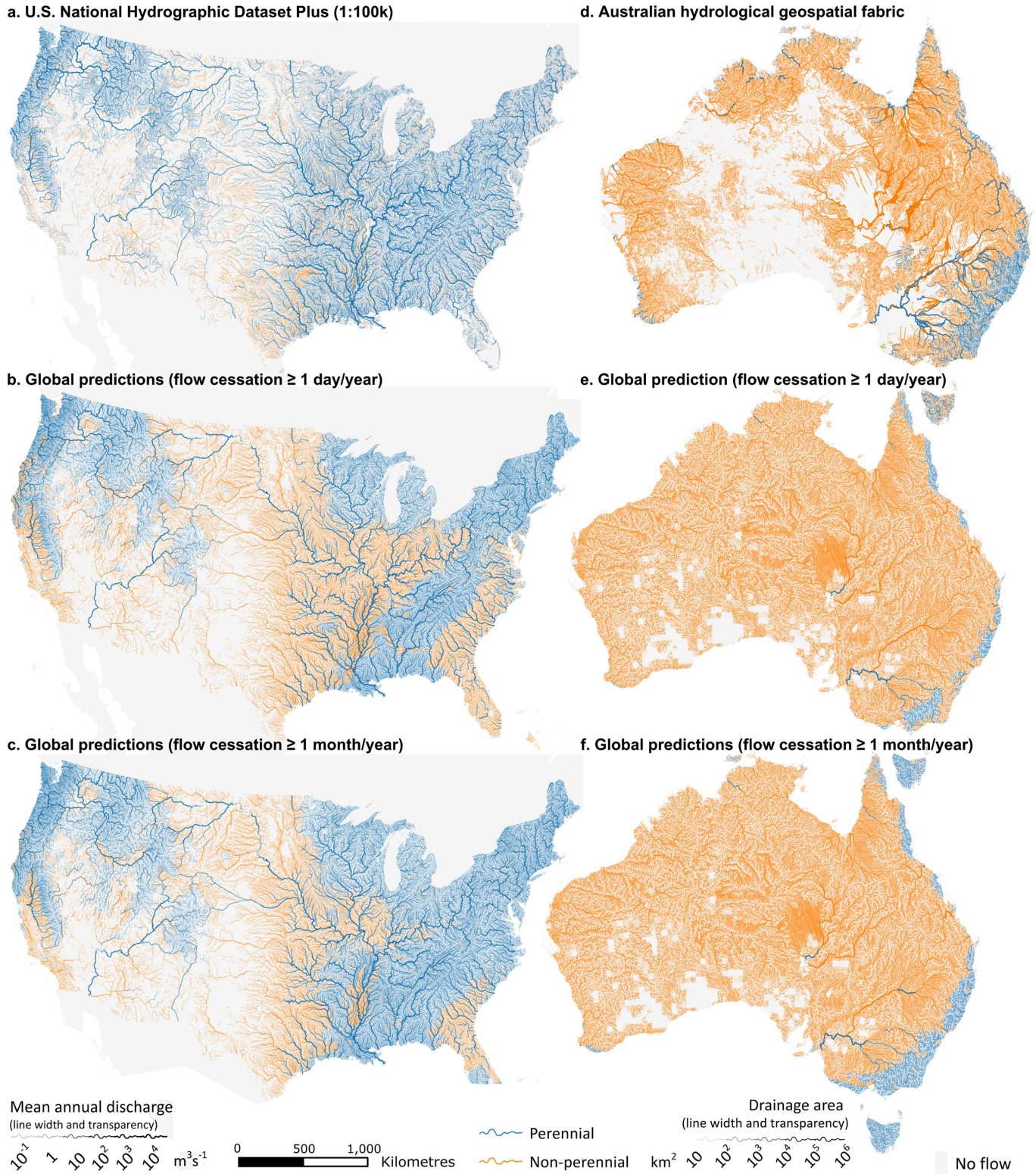

Extended Data Fig. 3 | Comparing global predictions to national maps of IRES in the USA and Australia. Comparison of **a**, the US National Hydrography Dataset (NHDPlus, medium resolution) and **d**, the Australian hydrological geospatial fabric, with our model predictions based on two thresholds of flow intermittence, either ≥1 zero-flow day per year (**b**, **e**), or ≥1 zero-flow month (30 days) per year (**c**, **f**), on average. Only rivers and streams with MAF ≥ 0.1 $m^3 s^{-1}$ are shown for the USA (**a**–**c**) and with drainage area ≥10 km^2 for Australia (**d**–**f**). The US reference dataset portrays 19–22% of the length of rivers and streams as non-perennial, depending on whether reaches without flow intermittence status are assumed to be perennial or removed; our estimates range from 51% (≥1 zero-flow day per year) to 36% (≥1 zero-flow month per year). We hypothesize that the remaining gap in IRES prevalence is attributable to a tendency of our model to overpredict intermittence across the eastern USA and an under-accounting of intermittence in medium to large rivers by the national dataset. The Australian reference dataset portrays 91% of the length of rivers and streams as non-perennial; our estimates range from 95% (≥1 zero-flow day per year) to 92% (≥1 zero-flow month per year). See Extended Data Fig. 7b for data sources. Mapping software: ArcMap (ESRI).

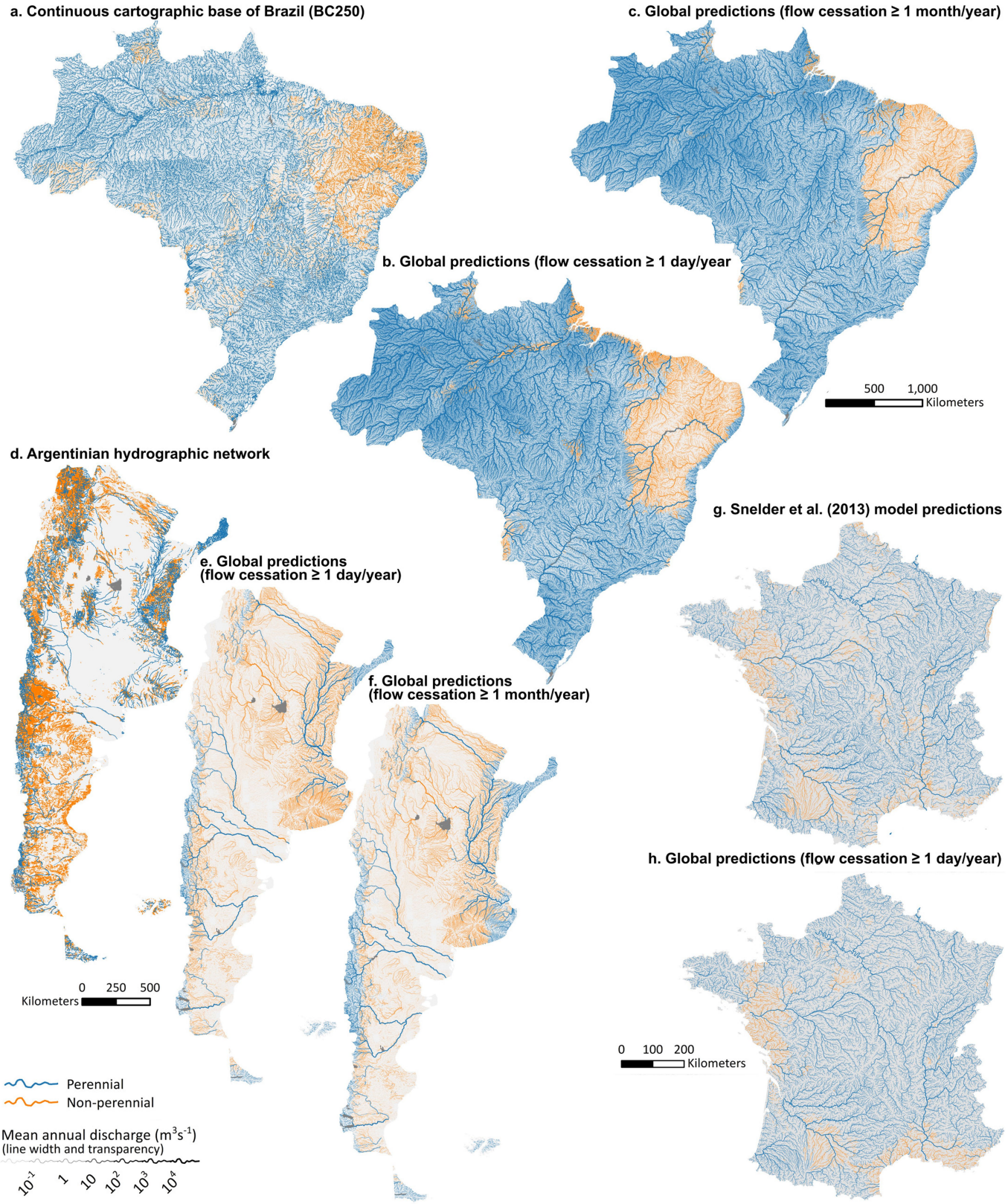

Extended Data Fig. 4 | See next page for caption.

Extended Data Fig. 4 | Comparing global predictions to national maps of IRES in Brazil, Argentina, and France. Comparison of **a**, the continuous cartographic base of Brazil (BC250), **d**, the Argentinian hydrographic network, and **g**, model predictions for France from Snelder et al.[21], with our model predictions based on two thresholds of flow intermittence, either ≥1 zero-flow day per year (**b**, **e**, **h**) or ≥1 zero-flow month (30 days) per year (**c**, **f**), on average. In **a** and **d**, only first-order streams (determined through network analysis) are visually differentiated (finer, semi-transparent lines), owing to the lack of a watercourse-size attribute in the Brazilian and Argentinian datasets. In **b**, **c**, **e**–**h**, only rivers and streams with MAF ≥ 0.1 $m^3 s^{-1}$ are shown. Snelder et al.[21] predict that 17% of the length of rivers and streams in France are non-perennial. We predict that 14% are non-perennial. This slight divergence may be partly driven by the difference in definition of flow intermittence: Snelder et al.[21] classified stations with ≥1 zero-flow day in the streamflow record as IRES whereas we used a threshold of 1 zero-flow day per year across the streamflow record. See Extended Data Fig. 7b for data sources. Mapping software: ArcMap (ESRI).

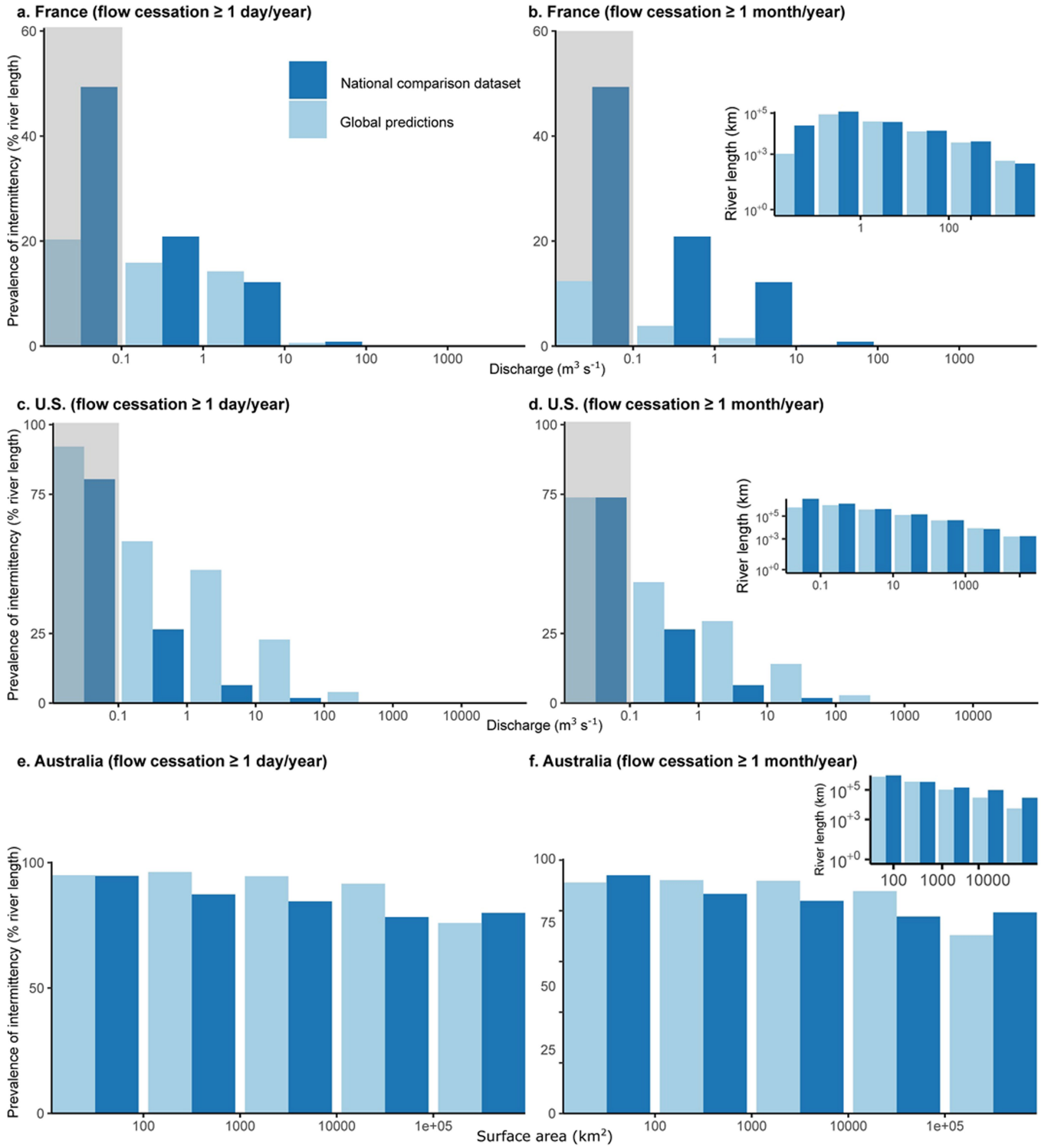

Extended Data Fig. 5 | Quantitative comparison between the predicted prevalence of flow intermittence and national estimates. **a**–**f**, Comparisons were conducted for France (**a**, **b**), the USA (**c**, **d**), and Australia (**e**, **f**), on the basis of two thresholds of flow intermittence, either ≥1 zero-flow day per year (**a**, **c**, **e**) or ≥1 zero-flow month (30 days) per year (**b**, **d**, **f**), on average. Bars for mapped rivers and streams with MAF < 0.1 $m^3 s^{-1}$ (for France and the USA) are greyed out as they were not included in the calculation of summary statistics. Inset graphs in **b**, **d**, **f** show comparisons of total river network length (log-transformed *y* axis), which in case of discrepancies can explain some of the differences in the predicted prevalence of intermittence.

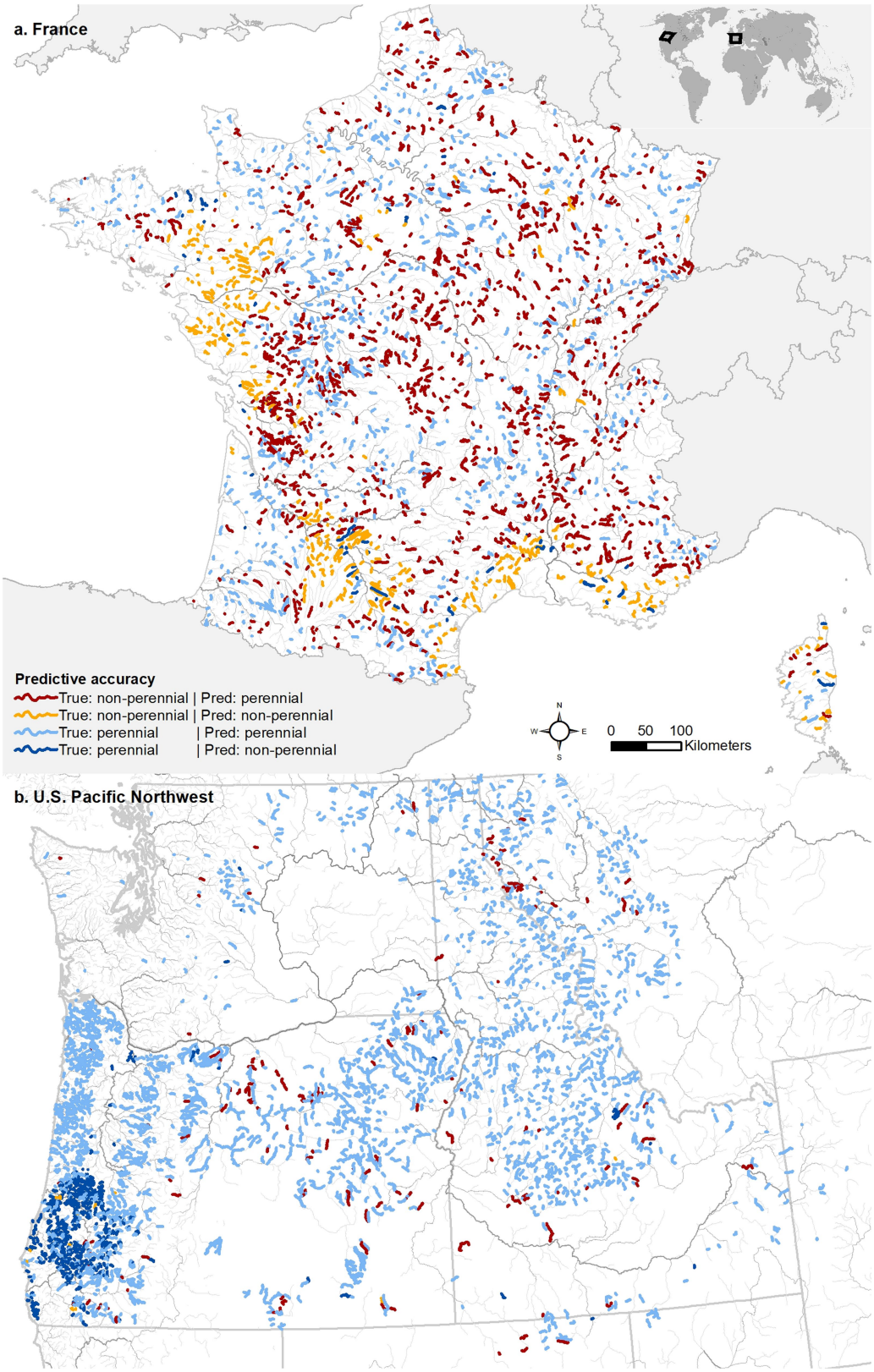

Extended Data Fig. 6 | Comparing global predictions to on-the-ground observations of flow cessation. a, **b**, Maps show individual RiverATLAS reaches and their predictive accuracy for France (**a**), and the US Pacific Northwest (**b**). Maps are drawn at identical cartographic scales. France (n = 2,297): balanced accuracy = 0.59, classification accuracy = 51%, sensitivity = 24%, specificity = 94%. US Pacific Northwest (n = 3,725): balanced accuracy = 0.47, classification accuracy = 80%, sensitivity = 10%, specificity = 83%. See Extended Data Fig. 7b for data sources. Mapping software: ArcMap (ESRI).

a

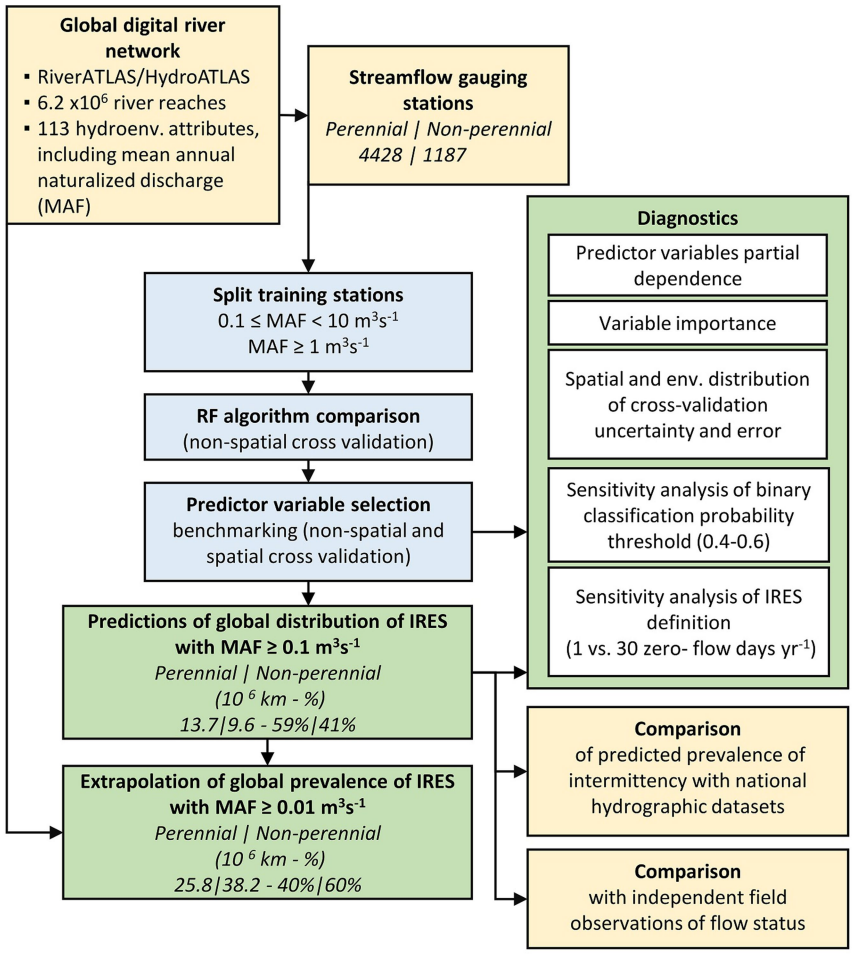

b

Theme	Region	Dataset – Source (access)	Scale
Streamflow gauging stations	World	In-situ river discharge data (as of 2014) - Global Runoff Data Center (GRDC)	-
	World	Global Streamflow Indices and Metadata Archive (GSIM) - Do et al. (2018) and Gudmunsson et al. (2018)	-
River network and attributes	World	HydroATLAS - Linke et al. (2019)	15 arc-second
National hydrographic data	Argentina	Aguas continentales de Argentina (cartografía básica de la república de Argentina) – Argentinian National Geographic Institute (IGN)	NA
	Brazil	Base Cartográfica Contínua do Brasil (BC250, 2019 version) - Brazilian Institute of Geography and Statistics (IBGE)	1:250k
	Australia	Australian Hydrological Geospatial Fabric (Geofabric, v. 3.2)	1:25-1:250k
	U.S.	National Hydrography Dataset Plus (NHDPlus, medium res., v.2)	1:100k
Previous model estimate	France	Snelder et al. (2013)	~1:25k
Point-based field observation data	U.S. Pacific Northwest	Streamflow observation points in the U.S. Pacific Northwest, 1977-2016 - McShane et al. (2017)	-
	France	Observatoire National des Etiages (ONDE eau, 2012-2019) – Office Français de la Biodiversité (OFB)	-
Population	World	Top-down unconstrained population estimates for individual countries – WorldPop	100 m

Extended Data Fig. 7 | Overview of study design and main data sources. **a**, Diagram of modelling workflow. **b**, Main data sources used in model development, predictions, diagnostics and comparisons. Data sources: Global Runoff Data Centre[53], Do et al.[54], Gudmundsson et al.[55], Linke et al.[27], Snelder et al.[21], McShane et al.[100], ONDE eau 2012–2019[101], National Hydrographic Data[102–105], WorldPop[90].

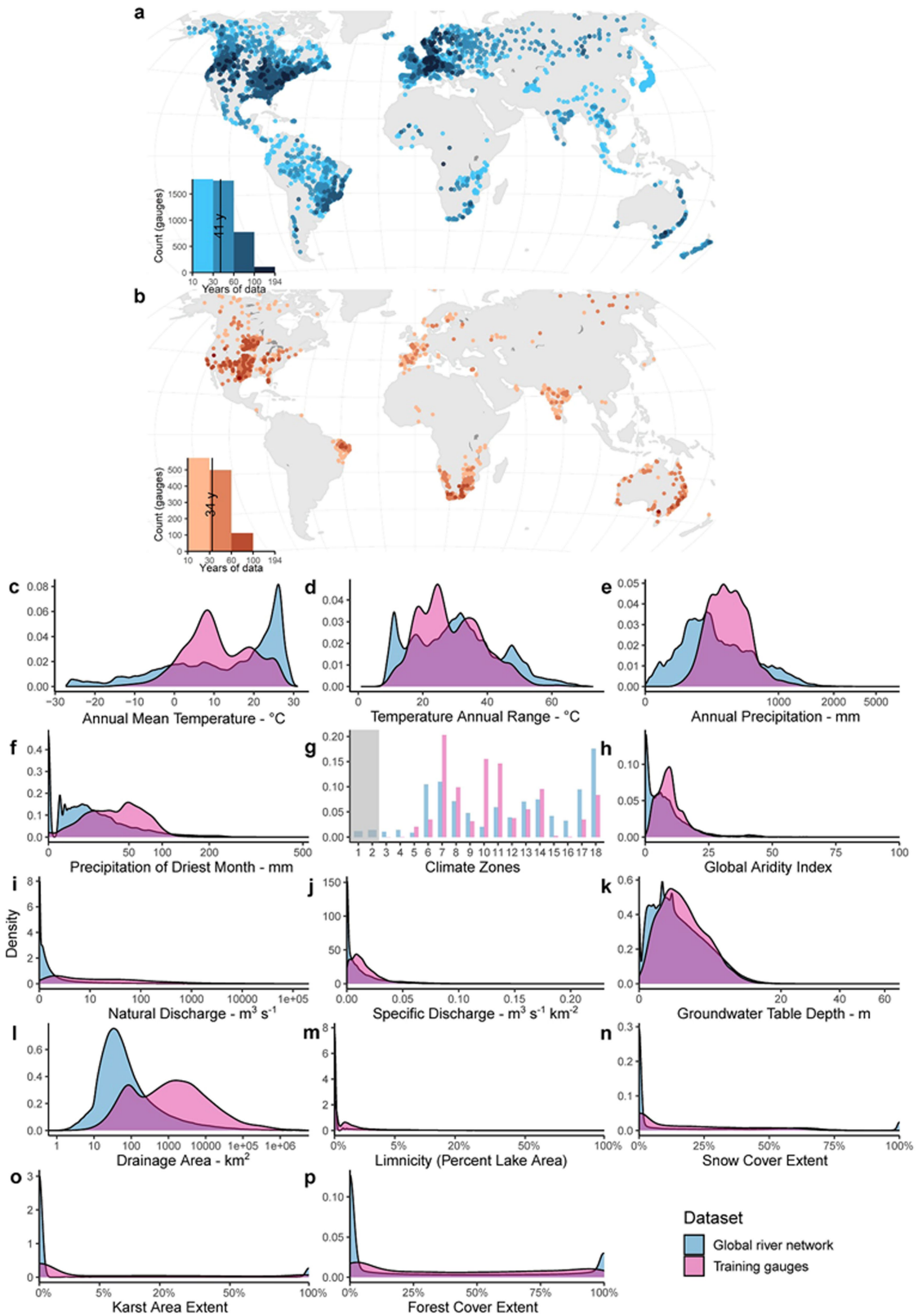

Extended Data Fig. 8 | See next page for caption.

Extended Data Fig. 8 | Spatial and environmental distribution of streamflow gauging stations used in model training and cross-validation. **a**, **b**, Gauging stations (n = 5,615) were deemed perennial (**a**) if their streamflow record included less than one zero-flow day per year, on average, across their record, or non-perennial (**b**) if they included at least one zero-flow day per year, on average, and at least one zero-flow day in every 20-year moving window across their record. Stations fulfilling neither condition **a** nor **b** were excluded. Darker points symbolize longer streamflow records. Only gauging stations with streamflow time series spanning at least 10 years were included in this analysis, excluding years with more than 20 missing days. **c**–**p**, Distribution of values for 14 hydro-environmental variables across the streamflow gauging stations used for model training/testing (purple, n = 5,615) and across all reaches of the global river network (blue, $n = 6.2 \times 10^6$). The distribution plots show empirical probability density functions (that is, the area under each density function is equal to one) for all variables, aside from climate zones (**g**) for which the relative frequency distribution is shown. All variables were averaged across the total drainage area upstream of the reach pour point associated with each gauging station or river reach, respectively. See Extended Data Table 2 for a description of the variables and Extended Data Fig. 1a for a description of the climate zones. No stations were available for climate zones Arctic 1 and Arctic 2. Mapping software: R statistical software (R Core Team).

Extended Data Table 1 | Definitions of commonly used terms for non-perennial rivers and streams

Term	Definition	Source
Non-perennial	Any lotic freshwater system that periodically ceases to flow and/or is dry at some point in time and/or space.	Busch et al., 2020[106]
Intermittent	A non-perennial river or stream with a considerable connection to the groundwater table, having variable cycles of wetting and flow cessation, and with flow that is sustained longer than a single storm event. These waterways are hydrologically gaining [surface water from groundwater] the majority of the time when considering long-term flow patterns.	Busch et al., 2020[106]
Ephemeral	A non-perennial river or stream without a considerable groundwater connection that flows for a short period of time, typically only after precipitation events. These waterways are hydrologically losing [surface water to groundwater] the majority of the time when considering long-term flow patterns.	Busch et al., 2020[106]
Intermittent rivers and ephemeral streams (IRES)	Flowing waters confined within a channel are called rivers or streams. Rivers are considered to be larger and deeper than streams, although the distinction is a loose one of common usage rather than based on fixed size and depth thresholds. The same common usage applies to describing differences in patterns of flow duration: the term 'ephemeral' implies a shorter duration and lower predictability than 'intermittent' — but again, there are no fixed boundaries. Therefore, given the broad association of channel size with flow duration, a stream is more likely to be ephemeral and a river to be intermittent, prompting the generalization.	Adapted from Datry et al., 2017[107]
Temporary	Rivers that cease to flow for a period of time during cycles of drying and rewetting.	Busch et al., 2020[106]

Refs. [106,107].

Extended Data Table 2 | Hydro-environmental characteristics used as candidate predictor variables in the split random forest model

Category	Attribute	Spatial	Aggregation	Source
Climate	Annual mean temperature (BIO1)	c, u	average	WorldClim v2[63]
Climate	Mean diurnal range (BIO2)	c, u	average	WorldClim v2[63]
Climate	Isothermality — (BIO2/BIO7) ×100 (BIO3)	c, u	average	WorldClim v2[63]
Climate	Temperature seasonality (SD ×100) (BIO4)	c, u	average	WorldClim v2[63]
Climate	Max. Temperature of warmest month (BIO5)	c, u	average	WorldClim v2[63]
Climate	Min. Temperature of coldest month (BIO6)	c, u	average	WorldClim v2[63]
Climate	Temperature annual range (BIO7)	c, u	average	WorldClim v2[63]
Climate	Mean temperature wettest quarter (BIO8)	c, u	average	WorldClim v2[63]
Climate	Mean temperature driest quarter (BIO9)	c, u	average	WorldClim v2[63]
Climate	Mean temperature warmest quarter (BIO10)	c, u	average	WorldClim v2[63]
Climate	Mean temperature coldest quarter (BIO11)	c, u	average	WorldClim v2[63]
Climate	Annual precipitation (BIO12)	c, u	average	WorldClim v2[63]
Climate	Precipitation of wettest month (BIO13)	c, u	average	WorldClim v2[63]
Climate	Precipitation driest month (BIO14)	c, u	average	WorldClim v2[63]
Climate	Precipitation seasonality (BIO15)	c, u	average	WorldClim v2[63]
Climate	Precipitation of wettest quarter (BIO16)	c, u	average	WorldClim v2[63]
Climate	Precipitation driest quarter (BIO17)	c, u	average	WorldClim v2[63]
Climate	Precipitation of warmest quarter (BIO18)	c, u	average	WorldClim v2[63]
Climate	Precipitation of coldest quarter (BIO19)	c, u	average	WorldClim v2[63]
Climate	Climate moisture index	c, u	annual min.	WorldClim v2 & Global-PET v2[63,64]
Climate	Climate zones	c	spatial majority	GEnS[32]
Climate	Global aridity index	c, u	average	Global Aridity Index v2[64]
Climate	Actual evapotranspiration	c, u	annual average	Global Soil-Water Balance[108]
Climate	Potential evapotranspiration	c, u	annual average	Global-PET v2[64]
Climate	Snow cover extent	c, u	annual average, max.	MODIS/Aqua[109]
Hydrology	Groundwater table depth	c	average	Global Groundwater Map[110]
Hydrology	Inundation extent	c, u	annual min., max.	GIEMS-D15[111]
Hydrology	Land surface runoff	c	annual average	WaterGAP v2.2[112]
Hydrology	Limnicity (percent lake area)	c, u	% extent	HydroLAKES[52]
Hydrology	Naturalized discharge	p	annual average, min, max, min/max, min/average	WaterGAP v2.2[112]
Hydrology	Runoff coefficient (runoff/precipitation)	c	average	WaterGAP v2.2[112], WorldClim v2[63]
Hydrology	Specific discharge (discharge/catchment area)	u	annual average, min.	WaterGAP v2.2[112]
Hydrology	Surface water dry period	c, u	average	GLAD[61]
Hydrology	Surface water high frequency	c, u	average	GLAD[61]
Hydrology	Surface water loss	c, u	average	GLAD[61]
Hydrology	Surface water maximum extent	c, u	average	GLAD[61]
Hydrology	Surface water permanent	c, u	average	GLAD[61]
Hydrology	Surface water seasonal	c, u	average	GLAD[61]
Hydrology	Surface water wet period	c, u	average	GLAD[61]
Landcover	Forest cover extent	c, u	% extent	GLC2000[113]
Landcover	Glacier extent	c, u	% extent	GLIMS[114]
Landcover	Land cover classes	c	spatial majority	GLC2000[113]
Landcover	Agricultural extent	c, u	% class 16	GLC2000[113]
Landcover	Permafrost extent	c, u	% extent	PZI[115]
Landcover	Potential natural vegetation classes	c	spatial majority	EarthStat[116]
Landcover	Pan, brackish/saline wetland extent	c, u	% class 7	GLWD[117]
Landcover	Intermittent wetland/lake extent	c, u	% class 9	GLWD[117]
Landcover	Wetland extent (incl. lakes, reservoirs, rivers)	c, u	% class group 1	GLWD[117]
Landcover	Wetland extent (excl. lakes, reservoirs, rivers)	c, u	% class group 2	GLWD[117]
Physiography	Drainage area	u	-	HydroSHEDS[50]
Physiography	Relative elevation [(average c elevation - average u elevation)/average u elevation]	(c-u)/u	average	EarthEnv-DEM90[118]
Physiography	Terrain slope	c, u	average	EarthEnv-DEM90[118]
Soils+Geology	Karst area extent	c, u	% extent	Rock Outcrops v3.0[119]
Soils+Geology	Lithological classes	c	spatial majority	GLiM[120]
Soils+Geology	Clay fraction in soil 0-100 cm	c, u	average	SoilGrids250m v2[62]
Soils+Geology	Sand fraction in soil 0-100 cm	c, u	average	SoilGrids250m v2[62]
Soils+Geology	Silt fraction in soil 0-100 cm	c, u	average	SoilGrids250m v2[62]
Soils+Geology	Soil water content	c, u	annual average, min.	Global Soil-Water Balance[108]

Spatial representations refer to: *p* (derived at the pour point of the river reach), *c* (derived within the local catchment that drains directly into the reach), or *u* (derived within the total drainage area upstream of the reach pour point). See ref. [27] for a full description of the methodology to calculate the variables.
Refs. [32,50,52,61–64,108–120].

Extended Data Table 3 | Performance summary of binary flow intermittence class predictions

a. Split model approach: twice-repeated 3-fold non-spatial cross-validation

Streamflow size class ($m^3 s^{-1}$)	Prediction (number of gauging stations) Non-perennial | Perennial		Total (N)	Prevalence of IRES (%) Pred. |True	Accuracy (%)	Sensitivity (%)	Specificity (%)	Precision (%)
	True: Non-perennial	True: Perennial						
(0, 0.1)	42 | 4	7 | 6	59	83 | 78	91	91	46	86
[0.1, 1)	292 | 55	44 | 504	895	38 | 39	89	84	92	87
[1, 10)	490 | 70	111 | 1217	1888	32 | 30	90	88	92	82
[10, 10^2)	175 | 24	82 | 1459	1740	15 | 11	94	88	95	68
[10^2, 10^3)	33 | 1	24 | 757	815	7 | 4	97	97	97	58
[10^3, 10^4)	1 | 0	2 | 187	190	2 | 1	99	100	99	33
≥ 10^4	0 | 0	0 | 28	28	0 | 0	100	-	100	-
All	**1033 | 154**	**270 | 4158**	**5615**	**23 | 21**	**92**	**87**	**94**	**79**

b. Split model approach: 40-fold spatial cross-validation

Streamflow size class ($m^3 s^{-1}$)	Prediction (number of gauging stations) Non-perennial | Perennial		Total (N)	Prevalence of IRES (%) Pred. |True	Accuracy (%)	Sensitivity (%)	Specificity (%)	Precision (%)
	True: Non-perennial	True: Perennial						
(0, 0.1)	43 | 3	9 | 4	59	88 | 78	80	93	31	83
[0.1, 1)	280 | 67	54 | 494	895	37 | 39	86	81	90	84
[1, 10)	459 | 101	151 | 1177	1888	32 | 30	87	82	89	75
[10, 10^2)	146 | 56	87 | 1454	1740	13 | 11	92	72	94	62
[10^2, 10^3)	14 | 20	16 | 765	815	4 | 4	96	41	98	47
[10^3, 10^4)	0 | 1	0 | 189	190	0 | 1	99	100	100	-
≥ 10^4	0 | 0	0 | 28	28	0 | 0	100	-	100	-
All	**939 | 248**	**317 | 4111**	**5615**	**22 | 21**	**90**	**80**	**93**	**75**

c. Single (non-split) model approach: twice-repeated 3-fold non-spatial cross-validation

Streamflow size class ($m^3 s^{-1}$)	Prediction (number of gauging stations) Non-perennial | Perennial		Total (N)	Prevalence of IRES (%) Pred. |True	Accuracy (%)	Sensitivity (%)	Specificity (%)	Precision (%)
	True: Non-perennial	True: Perennial						
(0, 0.1)	42 | 4	9 | 4	59	86 | 78	78	91	31	82
[0.1, 1)	303 | 44	64 | 484	895	41 | 39	88	87	88	83
[1, 10)	498 | 62	123 | 1205	1888	33 | 30	90	89	91	80
[10, 10^2)	166 | 33	62 | 1479	1740	13 | 11	95	83	96	73
[10^2, 10^3)	30 | 4	20 | 761	815	6 | 4	97	88	97	60
[10^3, 10^4)	1 | 0	1 | 188	190	1 | 1	99	100	99	50
≥ 10^4	0 | 0	0 | 28	28	0 | 0	100	-	100	-
All	**1040 | 147**	**279 | 4149**	**5615**	**23 | 21**	**92**	**88**	**94**	**79**

a–**c**, Tables show summary results for the split model approach based on a twice-repeated threefold non-spatial cross-validation (CV; **a**) and a once-repeated 40-fold spatial CV (**b**), as well as, for comparison, a single (non-split) model approach based on a twice-repeated threefold non-spatial CV (**c**). The colour coding mirrors Extended Data Fig. 2 with light colours slightly darkened for readability. The split model approach involves training two random forest sub-models with slightly overlapping MAF ranges, one trained to predict the streamflow intermittence probability of small-to-medium rivers with MAF < 10 $m^3 s^{-1}$ and the other for medium-to-large rivers with MAF ≥ 1 $m^3 s^{-1}$. Within the overlapping range of 1–10 $m^3 s^{-1}$ MAF, the average probability was calculated to avoid abrupt transitions at a singular size threshold. Gauging stations monitoring streams with a mean annual naturalized discharge <0.1 $m^3 s^{-1}$ were included in model training and testing (shown in grey font); however, no global model predictions were made below this discharge threshold. Sensitivity is the proportion of non-perennial reaches correctly classified as non-perennial. Specificity is the proportion of perennial reaches correctly classified as perennial. Precision is the proportion of reaches classified as non-perennial that are truly non-perennial. See Supplementary Fig. 3 and Supplementary Information section IV.b for the distribution of spatial cross-validation folds and details on the cross-validation procedure.